1

Advanced Ceramic Target Materials Produced by Self-Propagating High-Temperature Synthesis for Deposition of Functional Nanostructured Coatings - Part 1: Four Elements and Less Systems

Evgeny A. Levashov, Yury S. Pogozhev and Victoria V. Kurbatkina
National University of Science and Technology "MISIS", Russia

1. Introduction

An increase in the exploitation characteristics of various machines and tools is a key engineering–technical problem; solving it is directly associated with the introduction of new functional materials and coatings with improved properties. The industry of nanosystems is a high-priority branch in the development of science and technology that affects almost all scientific directions and spheres of activity.

Surface engineering, as applied to the fabrication of multifunctional nanostructured films (MNFs) whose characteristic crystallite size is from 1 nm to several tens of nanometers, plays an important role in the science of nanomaterials and nanotechnologies. The high volume fraction of interfaces with a strong bond energy, the absence of dislocations inside crystallites, the possibility of obtaining films with a controllable ratio of volume fractions of crystalline and amorphous phases, and the variation in the mutual solubility of the elements in interstitial phases are factors that lead to unique properties of nanostructured films and their multifunctionality which manifests itself in high values of hardness, elastic recovery, strength, thermal stability, heat resistance and corrosion stability. MNFs find application in the field of surfaces protection which are subjected to the simultaneous effect of elevated temperature, aggressive media, and various kinds of wear. These are, first and foremost, cutting and stamping tools; forming rolls; parts in aviation engines, gas turbines, and compressors; slider bearings; nozzles for the extrusion of glass and mineral fiber; etc. MNFs are also irreplaceable in the development of a new generation of biocompatible materials, namely, orthopedic implants, implants for craniofacial and maxillary surgery, fixations for the neck and lumbar spines, etc [1–3].

Currently, in order to obtain MNFs, chemical deposition methods, including plasma-activated methods, and physical deposition methods, such as magnetron sputtering, condensation with ion bombardment, and electron-beam and ion-beam sputtering, are widely used. The advantage of the magnetron sputtering technology is the insignificant heating of the substrate to 50–250°C [4]. This allows one to deposit a coating on almost any

material. In addition, hard and superhard MNFs with a different level of elastic–plastic characteristics can be deposited by this method [5].

The possibilities of magnetron sputtering can be substantially extended due to the use of composite multicomponent cathode targets obtained by self-propagating high-temperature synthesis (SHS) [6–8]. SHS-technology allows one to produce a wide spectrum of targets based on ceramics, metal ceramics, and intermetallic compounds. One fundamental distinction of sputtering processes of composite and metal targets is in fact that, in the former case, the substance is transported by the uniform flow of metal and nonmetal atoms and ions. In this case, all elements necessary for the formation of the coating, including nonmetal coatings (C, O, N, P), can be sputtered from one target [9, 10]. In sputtering installations, both the disc and planar–extended rectangular segment SHS targets can be used [11].

The SHS targets passed successful tests in various types of installations, namely, dc magnetron systems (MS) [1, 9, 12–14, 15–17, 18–24], high-frequency [25] and pulsed MS [11], MS with additional inductively coupled plasma [26], and arc evaporators [27].

Over the last several years, using the magnetron sputtering of SHS targets, hard coatings were obtained in the systems Ti–Si–N [9, 12, 28], Ti–B–N [10, 13, 29, 30], Ti–Si–B–N [4, 13, 29], Ti–Si–C–N [13, 29], Ti–Al–C–N [13, 29], Ti–C–N [31], Ti–Mo–C–N [31], Ti–Al–B–N [32], Ti–Al–Si–B–N [17, 18, 30], Ti–Cr–B–N [10, 12, 14, 17, 30], Cr–B–N [10, 12, 33, 34], Ti–Zr–C–O–N [19], Ti–Ta–Ca–P–C–O–N [23, 24], Ti–Cr–Al–C–N [35, 36], etc.

Taking into account the increase in demand for various compositions of composite targets, we decided that it is important to present the data on the features of the synthesis of the most interesting and necessary classes of SHS targets differing in regards to their combustion mechanisms and structure formation in the form of the review. In this work, we present both recently obtained results and those that we have not yet published.

2. Ceramic materials in system Ti-Cr-Al-C

Let us consider the class of refractory oxygen-free compounds possessing a layered structure and a unique combination of metal and ceramic properties, which are generally described by the formula $M_{n+1}AX_n$, where M is the transition metal, A is the preferentially subgroup IIIA or IVA element of the periodic table, and X is carbon or nitrogen [37]. They are characterized by a low density; high thermal conductivity, electrical conductivity, and strength; reduced (when compared with ceramic materials) elasticity modulus; excellent corrosion resistance in aggressive external media; resistance to high-temperature oxidation; and resistance to thermal shocks. However, due to their layered structure and by analogy with hexagonal boron nitride and graphite, these materials are easily subjected to mechanical treatment [38]. Like ceramics, they have a high melting point, and they are sufficiently stable at elevated temperatures up to 2000°C [39].

The main problem in obtaining the $M_{n+1}AX_n$ phases (MAX phases) is that the final products contain impurity phases (for example, TiC, $TiAl_3$, Cr_2Al, Cr_7C_3, etc), which exert a substantial effect on the exploitation characteristics of the ceramic material. The main cause of the phase nonuniformity in the synthesis of similar compounds is multistage solid-phase interaction, when thermodynamically stable compounds such as titanium carbide are formed during intermediate stages. In addition, local violations in the stoichiometric composition take place. They are associated, for example, with the partial evaporation of aluminum at high temperatures. However, we can confidently predict that using various

methods to obtain them, as well as varying the phase and granulometric compositions of the starting components of the mixture, allows one to extend the range of exploitation properties and the usage region of the $M_{n+1}AX_n$ -based materials.

The works devoted to the use of the SHS method to fabricate $M_{n+1}AX_n$ -based materials in the Ti_3AlC_2 [10, 11], Ti_2AlC [12, 13], and Cr_2AlC ternary systems [2, 14, 40] and in the $Ti_{2-x}Cr_xAlC$ quaternary system [41, 42] are well known. An investigation of the features of the structural and phase formation of the SHS compact synthesis products, depending on the preparation method of the reactionary mixture and the ratio of main reagents (titanium, chromium, aluminum, and carbon), remains topical.

To obtain new composite materials (CM), we used the technology of the forced SHS pressing based on the sequential performance of the SHS and pressing of hot products of the synthesis to the virtually pore-free state. We used PTS titanium powders (TU (Technical Specifications) 14-1-3086-80), PH-1S chromium powders (GOST (State Standard) 5905-79), ASD-1 aluminum powders (TU-48-5-226-87), and P804T ash (TU 38-1154-88) as starting mixture components.

All the compositions of the materials under study in this work are described by the general formula $Ti_{2-x}Cr_xAlC$, where x is the mixture parameter. The experimental compositions of the powder mixtures are presented in Table 1.

Experimental sample	X	Content of initial components, wt %			
		Ti	Cr	Al	C
Ti_2AlC	0	69,7	-	21,6	8,7
$Ti_{1,5}Cr_{0,5}AlC$	0,5	51,5	18,6	21,3	8,6
TiCrAlC	1	33,8	36,7	21,0	8,5
$Ti_{0,5}Cr_{1,5}AlC$	1,5	16,7	54,1	20,8	8,4
Cr_2AlC	2	-	71,3	20,5	8,2

Table 1. Composition of the green mixtures

The procedures for preparing and investigating the experimental samples, as well as a description of the equipment that was used, are presented in detail in [41], where the mechanism of the phase and structure formation of the synthesis products in the ternary (Ti–Al–C) and quaternary (Ti–Cr–Al–C) systems was also investigated. Using a differential thermal analysis, two main stages of formation of complex carbides in the Ti–Al–C system upon heating in a temperature range of 298–1673 K are revealed.

The first stage is associated with the formation of the Ti_yAl_z intermetallic compounds according to the general formula

$$yTi + zAl \rightarrow Ti_yAl_z, \quad (1)$$

and titanium carbide is formed at the second stage with its subsequent interaction with the intermetallic compounds and aluminum melt with the formation of the $Ti_{y+1}AlC_z$ ternary compounds:

$$TiC_y + Ti_yAl_z \rightarrow Ti_{y+1}AlC_z, \quad (2)$$

$$TiC_y + Al \rightarrow Ti_{y+1}AlC_z. \quad (3)$$

The mechanism of formation of the $Ti_{y+1}AlC_z$ compounds during the synthesis in the combustion mode somewhat differs from that described above, which is associated with the higher combustion rate (U_c) and temperature (T_c). Since under the initial conditions $T_0 = T_{room}$, the adiabatic temperature (T_c^{ad} = 1773 K) is lower than the melting point of titanium (1933 K) and its interaction with carbon proceeds through the aluminum melt (liquid phase), which is, in essence, the "diffusion accelerator" in this case. When using the "chemical heater" (the mixture of the Ti, B, and C powders), T_0 increases, which is accompanied by an increase in T_c^{ad} to 2290 K (Table 2). After melting titanium, the reaction surface is formed via spreading of the Ti–Al melt over the ash surface, carbon is saturated by this melt, and titanium carbide grains are isolated from it. In this case, the $Ti_{y+1}AlC_z$ phases are formed from the melt at the stages of both the primary and secondary structure formation.

Experimental sample	X	T_0, K	U_c, cm/s	T_c^{ad}, K	T_c^{ad*}, K
Ti_2AlC	0	1000	2.1	1775	2282
$Ti_{1,5}Cr_{0,5}AlC$	0,5	1050	1.5	1773	2290
TiCrAlC	1	1100	0.9	1776	2289
$Ti_{0,5}Cr_{1,5}AlC$	1,5	1550	1.5	1235	2284
Cr_2AlC	2	2100	1.8	861	2157

Note: T_c^{ad*} is the adiabatic temperature of the combustion allowing for the heat release from the "chemical heater" necessary for the steady-state mode of combustion.

Table 2. Combustion parameters

It is evident from the data of Table 2 that the adiabatic combustion temperature of the mixtures calculated by the THERMO program is almost identical for the formation of Ti_2AlC, $Ti_{1.5}Cr_{0.5}AlC$, and TiCrAlC. As the chromium content in the mixture increases (the compositions $Ti_{0.5}Cr_{1.5}AlC$ and Cr_2AlC), the temperature decreases. It's addition also exerts a similar effect on the combustion rate. The maximal value of U_c (2.1 cm/s) is observed for the synthesis of Ti_2AlC. The introduction of the chromium powder into the green mixture to the molar ratio Ti : Cr = 1 : 1 causes a decrease in U_c to 0.9 cm/s, while an increase in the initial SHS temperature is favorable to an increase in the combustion rate during the synthesis of $Ti_{0.5}Cr_{1.5}$ AlC and Cr_2AlC to 1.5 and 1.8 cm/s, respectively.

The results of an X-ray phase analysis of the products are presented in Table 3 [41]. At x = 0, they include two types of the $M_{n+1}AX_n$ phases, namely, Ti_3AlC_2 (80%) and Ti_2AlC (16%) with the hexagonal crystal lattice. Both phases are formed as a result of the chemical interaction between titanium carbide and the melt of aluminum and titanium. Analogously to [46], the products also contain a small amount (4%) of nonstoichiometric titanium carbide TiC_y with the lattice constant 0.4312 nm and traces of free aluminum (~1%), the presence of which indicates the incomplete transformation by reactions (2) and (3) due to the multistage solid-phase interaction of thermodynamically stable compounds.

Upon the introduction of the chromium powder into the initial mixture to the molar ratio Ti: Cr = 1.5:0.5 (x = 0.5), the $M_{n+1}AX_n$ phase with the stoichiometric composition Ti_3AlC_2 is formed in an amount of 52% with the lattice constant somewhat increased compared with the phase of the same composition at x = 0. The lattice constant of titanium carbide also increases in this case, which is associated with the formation of complex titanium–chromium carbide (Ti,Cr)C in the combustion wave due to the partial substitution of

titanium atoms in the TiC lattice by the Cr atoms. This complex carbide then interacts with the Ti–Al melt with the formation of the $M_{n+1}AX_n$ phase with an increased lattice constant. In addition to the main phases, chromium aluminide Cr_4Al_9 (12%), which is usually present as the intermediate phase, is found in the product [42, 43].

The synthesis products at x = 1 possess the largest distinction with respect to the phase composition compared with other materials under study. It is evident from Table 3 that their main phases are TiC, Cr_4Al_9, and Cr_2Al, while the content of the $(Cr,Ti)_2AlC$ phase is only 8%.

Experimental sample	X	Phase composition	Amount of the phase, wt %	Lattice constant, nm
Ti_2AlC	0	TiC	4	A = 0,4312
		Ti_3AlC_2	80	A = 0,3069 C = 1,8524
		Ti_2AlC	16	A = 0,3062 C = 1,3644
$Ti_{1,5}Cr_{0,5}AlC$	0,5	TiC	36	A = 0,4322
		Ti_3AlC_2	52	A = 0,3071 C = 1,8556
		Cr_4Al_9	12	A = 0,9054
TiCrAlC	1	TiC	66	A = 0,4314
		$(Cr,Ti)_2AlC$	8	A = 0,2866 C = 1,2867
		Cr_4Al_9	20	A = 0,9040
		Cr_2Al	6	A = 0,2997 C = 0,8709
$Ti_{0,5}Cr_{1,5}AlC$	1,5	TiC	19	A = 0,4308
		$(Cr,Ti)_2AlC$	54	A = 0,2864 C = 1,2833
		Cr_2Al	22	A = 0,3005 C = 0,8677
		Cr_7C_3	5	A = 0,4517 B = 0,7015 C = 1,2167
Cr_2AlC	2	Cr_2AlC	98	A = 0,2858 C = 1,2815
		Cr_7C_3	2	A = 0,4517 B = 0,7014 C = 1,2166

Table 3. Results of an X-ray phase analysis of the synthesis products in the Ti–Cr–Al–C system

With a further increase in the chromium concentration in the mixture (x = 1.5), the $M_{n+1}AX_n$ phase of the $(Cr,Ti)_2AlC$ composition (54%) is formed. In this case, the content of titanium carbide decreases to 19% upon an increase in the content of chromium aluminide Cr_2Al to 22%, which also indicates the incompleteness of diffusion in the combustion wave. It should

be noted that the largest amount of chromium carbide Cr_7C_3, which is less stable than the $M_{n+1}AX_n$ phase, is present in this sample. Its presence leads to the embrittlement of the material and the worsening of its strength characteristics; therefore, it is undesirable.

The results of an X-ray phase analysis of the synthesis products at x = 2 showed that they are virtually single-phase and include 98% Cr_2AlC.

Thus, the highest content of the $M_{n+1}AX_n$ phase is achieved for the samples corresponding to the stoichiometric compositions Ti_2AlC and Cr_2AlC, in which only one main element, namely, titanium or chromium, is present.

Figure 1 shows the microstructures of the fractures of the material under study in the Ti–Cr–Al–C system. They are similar for all the alloys (Figs. 1a, 1b, 1d, 1e), except for the sample synthesized at x = 1.

The microstructure of the Ti_2AlC product obtained from the chromium-free mixture at x = 0 preferentially consists of two types of $M_{n+1}AX_n$ phases, namely, Ti_3AlC_2 and Ti_2AlC, which have a characteristic layered (terrace) structure with a small amount of rounded TiC grains (Fig. 1a) with an average particle size of ~3 μm. A more detailed investigation of the alloy microstructure showed [38, 41] that the grains of the $M_{n+1}AX_n$ phases consist of numerous 100–300 nm thick layers (Fig. 2a).

The structure of the products at x = 0.5 differs somewhat from the sample containing no chromium. Here, we clearly observe rounded TiC grains with an average size of 1.5 μm, as well as the inclusions of the Cr_4Al_9 phase (Fig. 1b). The content of the $M_{n+1}AX_n$ phase is lower in this case.

The largest structural distinctions are characteristic of the sample with the molar ratio Ti:Cr = 1:1 (see Fig. 1c). Here, the main phase is titanium carbide with an average grain size of 0.5 μm. In addition, chromium aluminide is observed and, in a small amount, $(Cr,Ti)_2AlC$.

We also found the grains of the $(Cr,Ti)_2AlC$ phase with a characteristic laminate structure in the structure of the alloy at x = 1.5. They are surrounded by grains of titanium carbide, chromium aluminide Cr_2Al, and a small amount of chromium carbide Cr_7C_3 (see Fig. 1d).

Figure 1e shows the microstructure of the synthesis products at x = 2. It is evident that the material under study is highly structurally uniform and almost completely consists of grains of the Cr_2AlC phase with different spatial orientations. However, Cr_7C_3 inclusions are sometimes present on their surface; their amount is ~2%.

Taking into account the positive experience of applying mechanical activation (MA) to the problems of increasing the transformation depth and structural and phase uniformity of the combustion product [44–47], in order to increase the content of the MAX phases, the green mixtures were subjected to MA in a planetary mill. According to the results of our studies, it was established that MA provides an increase in the content of the MAX phases.

In Table 4, the green mixture prepared in a ball mill without MA by procedure [41] is denoted as the NA, while the mixtures after mechanical activation in various modes are denoted as MA1, MA2, and MA3. For example, if the fraction of the MAX phase in the sample with x = 1 was no higher than 8% [41], then it increased to 45% after MA3 (for 60 min). This effect is due to the complex influence of MA on the structure, properties, and reactivity of the mixture.

As shown above, the chromium addition into the Ti–Al–C mixture complicates the synthesis of the materials, which takes place firstly because the Cr_2AlC phase has a very low adiabatic combustion temperature (see Table 2). For this reason, we failed to implement SHS in the mixtures with x = 1 and 2 at the initial temperature close to room temperature. The mechanical activation allowed us to increase the reactivity of green mixture. A special series

of experiments on determining the combustion temperature of the ternary and quaternary MA mixtures was devoted to this problem. It was established that, at T_0 = 295 K, only MA mixtures with a high titanium content (x = 0 and 0.5) burn. We also failed to achieve SHS at room temperature in the MA mixtures with x = 1.0, 1.5, and 2.0.

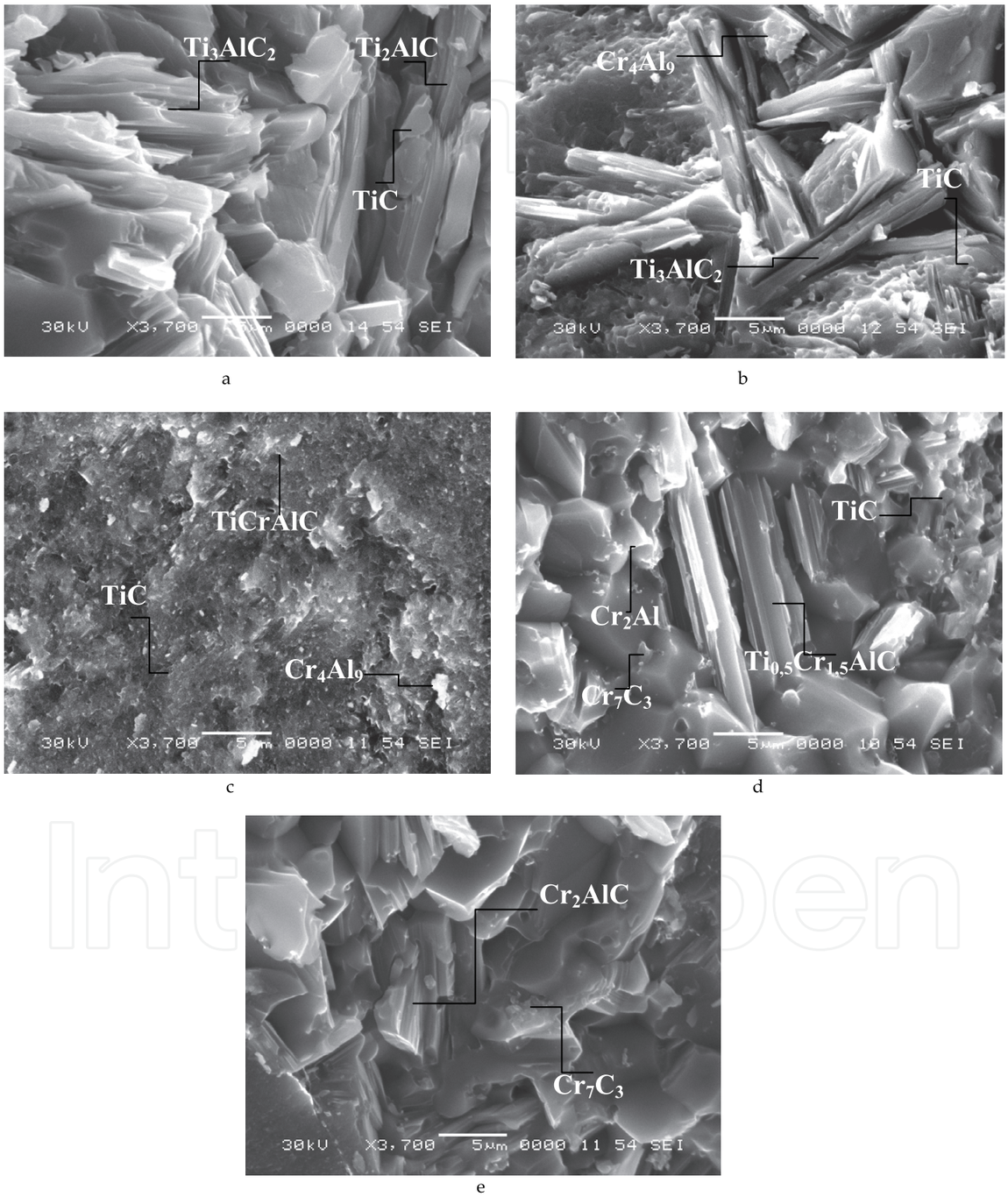

Fig. 1. Microstructure of the synthesis products in the Ti–Cr–Al–C system at various values of the mixture parameter x = (a) 0, (b) 0.5, (c) 1.0, (d) 1.5, and (e) 2.0.

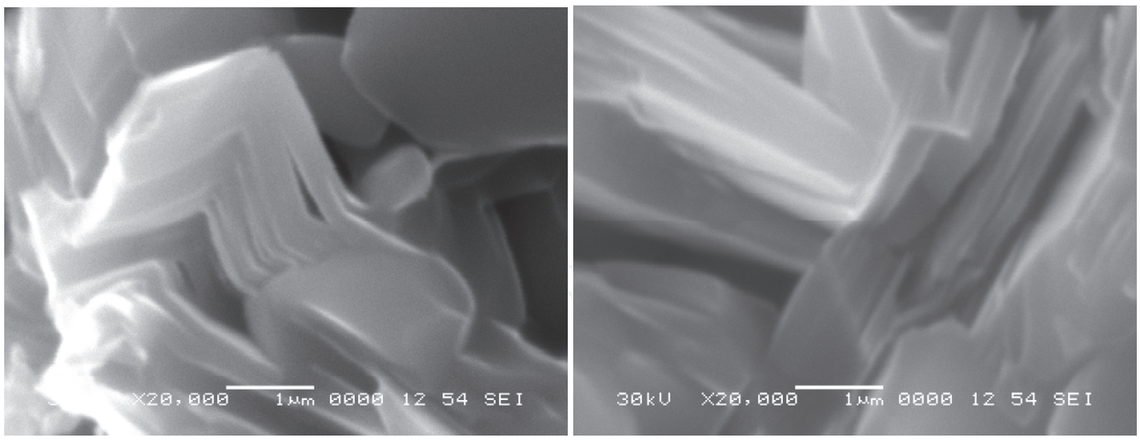

a b

Fig. 2. Microstructure of the Ti_2AlC (a) alloy and Cr_2AlC (b) alloy.

When analyzing the known mechanisms of formation of the MAX phases [38, 39, 41], as well as allowing for the combustion experiments, we can assume that these phases are formed due to the solid-phase diffusion. In this case, the structural factors are of importance, namely, the phase size and the component distribution throughout the mixture volume. We selected the MA modes starting from this point. The contribution of MA to the ternary mixtures with x = 2 (Cr_2AlC) and x = 0 (Ti_2AlC) consisted of intensifying the phase content and increasing the fraction of Ti_2AlC from 16 to 73%. The largest effect was observed for quaternary mixtures with x = 1.5, 1.0, and 0.5. Figure 3 shows the morphology of the starting reagents, and Fig. 4 shows the structure of the mixture with x = 0.5 after MA. The nonactivated mixture consists of the dissimilar Ti, Cr, and Al powders and ash with the scale of the heterogeneity scale close to the characteristic size of metal particles.

After 28 min long MA, the mixture structure undergoes substantial variations. Due to intense plastic deformation, agglomerated particles with a layered structure (Fig. 4a, point 1) appear. They are based on the mixed Ti and Cr layers, while Al and C are distributed over the surface of the layers. However, the number of the layered particles after MA is small. Most of them are the deformed particles of the starting chromium and titanium powders (see Fig. 4a, points 2 and 3). As the MA time increases to 60 min, the fraction of the agglomerated particles reaches 90–95%, while the average agglomerate size decreases to 10 μm (Fig. 4b). The separate layers are not thicker than several micrometers.

The structural variations in the mixture substantially affect the phase composition of the synthesis products. This is evident from Table 4, in which the composition of the samples is obtained by SHS pressing technology from the preliminarily activated mixtures by the modes providing the maximal amount of the MAX phase in the final product.

It is noteworthy that, depending on the MA mode, we can obtain composite materials with different compositions. Figure 5 shows the microstructures of mixtures with x = 1.5 obtained under various MA modes and the corresponding compositions of the SHS products. According to MA1 and MA3 modes, all the components are charged simultaneously and activated in a planetary mill for 18 and 60 min, respectively. Sequential charging is performed in the MA2 mode. Initially, chromium is activated with carbon and then titanium and aluminum are sequentially added. Similarly to MA1, the total duration of the treatment is 18 min. The structure of the mixture in the MA1 mode contains uniaxial agglomerates

Experimental sample	X	Mixture preparation	Content of the phases after SHS pressing, wt %	$\sigma_{bend.}$, MPa	E, GPa	HV, GPa	ρ_t, g/cm^3	$P_{res.}$, %
Ti_2AlC	0	NA	Ti_2AlC - 15 Ti_3AlC_2 -80 TiC -4 Al - 1	312	477	4,4	3.90	11,2
		MA1	Ti_2AlC - 73 Ti_3AlC_2 - 16 TiC - 2 Ti Al_2 - 9	388	386	3.9	4,1	7,2
		MA2	Ti_2AlC - 30 Ti_3AlC_2 65 TiC - 5	401	443	5,5	4,15	5,8
$Ti_{1,5}Cr_{0,5}AlC$	0,5	NA	Ti_3AlC_2 - 52 TiC - 36 Cr_4Al_9 - 12	286	434	5,7	4.30	5,5
		MA2	Ti_3AlC_2- 55 $(TiCr)_2AlC$ - 2 TiC - 29 Cr_4Al_9 - 7 Cr_2Al - 7	254	517	4,7	4,40	6,5
TiCrAlC	1	NA	$(Cr,Ti)_2AlC$ -8 TiC - 66 Cr_4Al_9 - 20 Cr_2Al - 6	129	438	13,5	4,70	4,1
		MA3	$(Cr,Ti)_3AlC_2$ - 45 TiC - 43 Cr_4Al_9 - 12 Cr-Ti - 1	137	334	7.5	4,40	5,4
$Ti_{0,5}Cr_{1,5}AlC$	1,5	NA	Cr_2AlC - 54 TiC - 19 Cr_7C_3 - 5 Cr_2Al - 22	222	507	7,1	5.00	4,9
		MA3	Cr_2AlC - 17 $(Ti,Cr)_3AlC_2$ - 60 $(Cr,Ti)_2AlC$ - 23	383	441	5.1	4,42	4,3
Cr_2AlC	2	NA	Cr_2AlC - 98 Cr_7C_3-2	459	573	4,7	4.90	4,7
		MA1	Cr_2AlC-100	462	516	4,0	5,02	6,8

Note: σ_{bend} is the ultimate bending strength, E is the elasticity modulus, HV is the Vickers hardness, ρ_t is the true density determined using the helium pyknometer, and P_{res} is the residual porosity.

Table 4. Phase composition and physical and mechanical properties of the synthesis products in the Ti–Cr–Al–C system

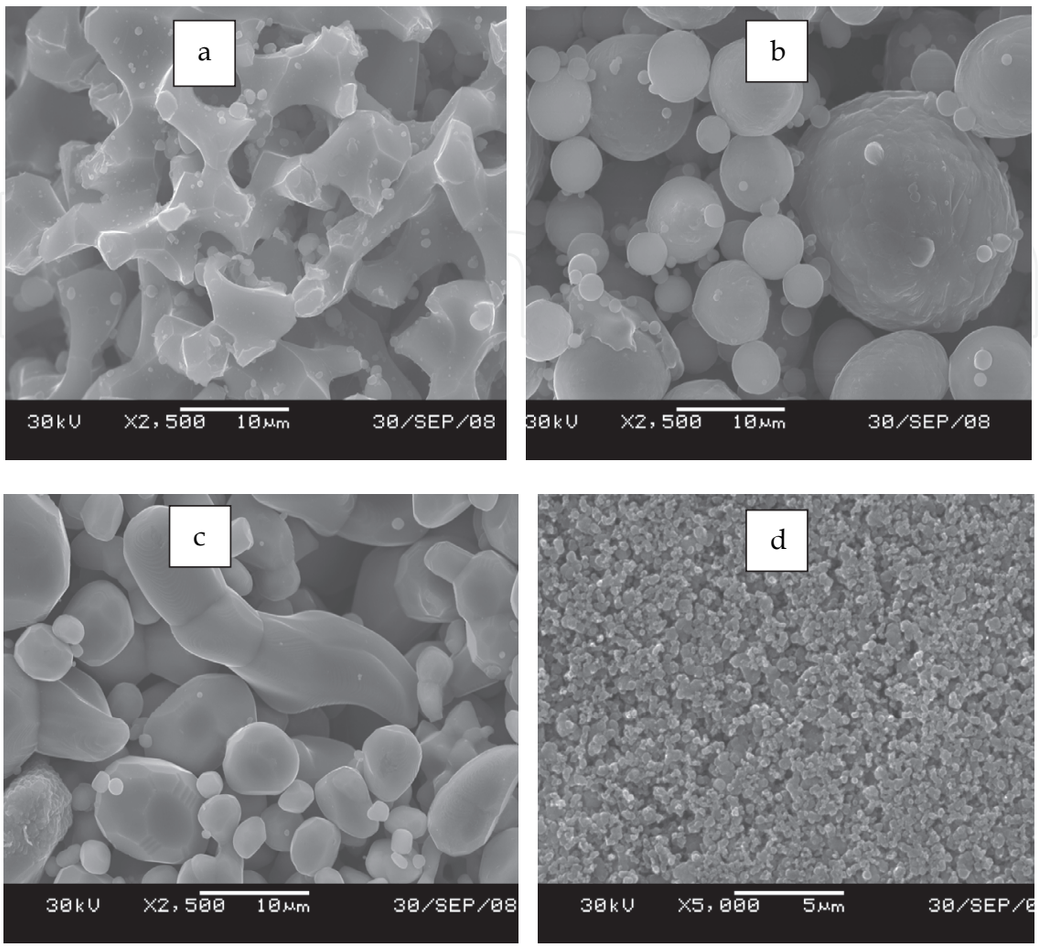

Fig. 3. Structures of the initial powders: (a) the PTS titanium, (b) the ASD_1 aluminum, (c) the PKh-1S chromium, and (d) the P804T ash.

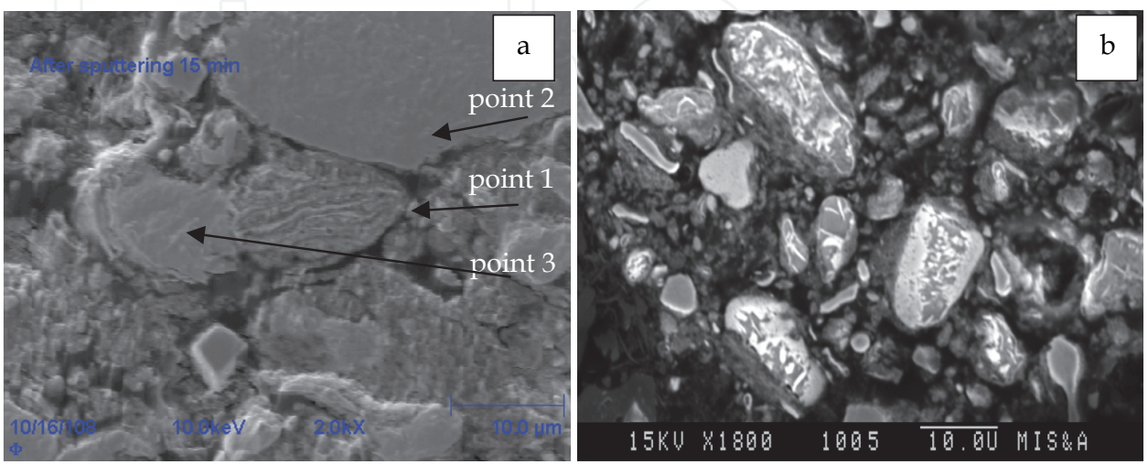

Fig. 4. Structure of the green mixture at x = 0.5 after MA for 28 min (a) and 60 min (b).

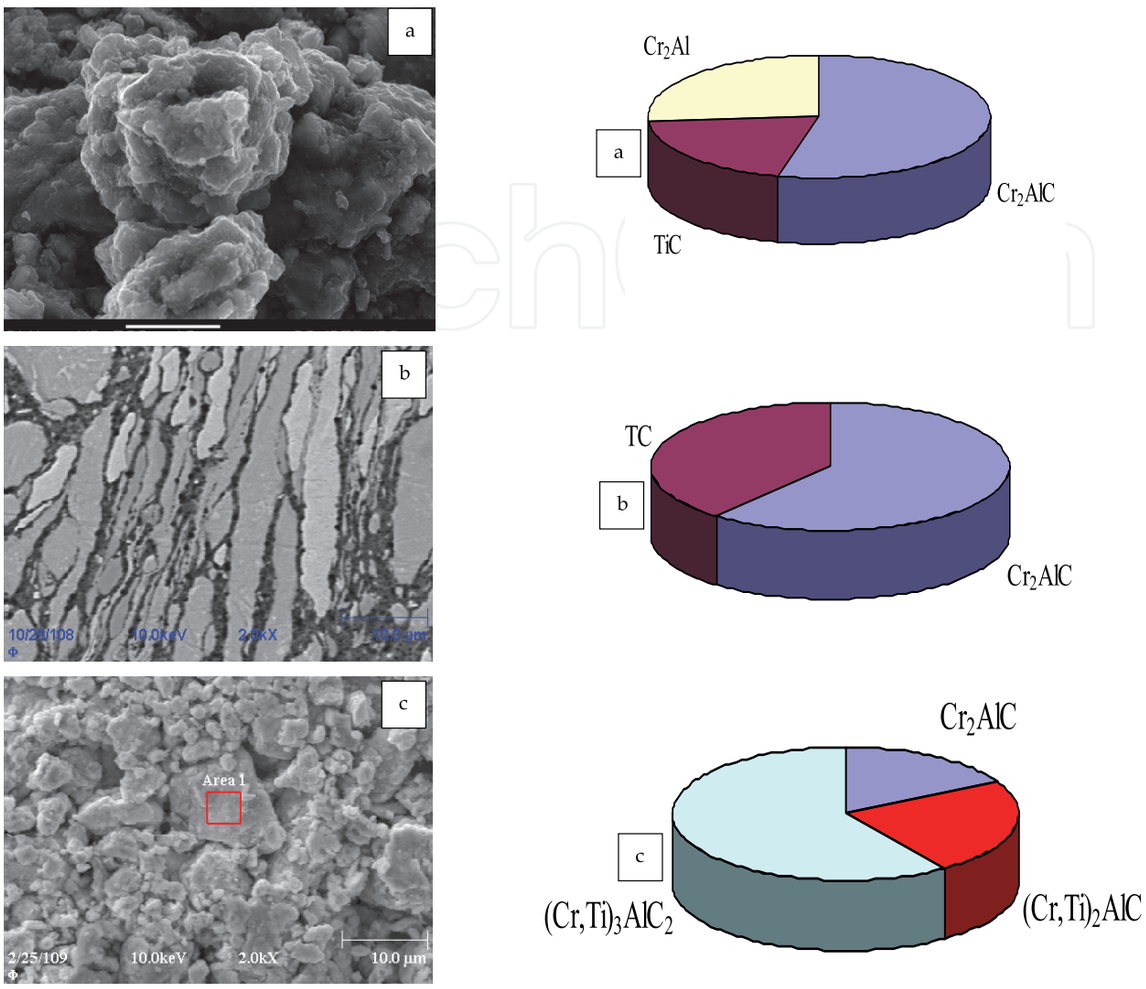

Fig. 5. Structure of the mechanically activated mixture (x = 1.5) and the composition of synthesis products. MA1 (a), MA2 (b), and MA3 (c).

with an average size of >10 µm (see Fig. 5a). The layered structure is observed for the agglomerates in the MA2 mode (see Fig. 5b). The thickness of titanium and chromium layers is from 2 to 10 µm that of aluminum is less than 0.5–1.0 µm, and that of carbon (ash) is less than 100 nm. In the MA3 mode, the mixture has a fine well-mixed structure. The average size of the agglomerates is 10–20 µm, and the size of particles or layers is mostly <1.0 µm. The amount of agglomerated particles is ~90–95% of their total amount. In the first case, the main phase of the synthesized products is Cr_2AlC (54%), although the TiC (21%) and Cr_2Al (23%) are also present. In the second case, chromium aluminide is absent; the Cr_2AlC content increases to 66%, and that of TiC increases to 34%. In the MA3 mode, the sample consists of three MAX phases: $(Cr,Ti)_3AlC_2$, Cr_2AlC, and $(Cr,Ti)_2AlC$. As is evident from the data of Table 4, none of considered MA modes allowed us to obtain samples completely consisting of MAX phases for the mixture with x = 0.5. The maximal amount of the Ti_3AlC_2 phase was 55%. In addition, TiC and chromium aluminides are always present the samples. A similar situation is also observed for the mixture with x = 1. The $(Cr,Ti)_3AlC_2$ content does

not exceed 50%. It is possible that the phase composition is close to the equilibrium composition for these mixture compositions.

As is evident from the data of Table 4, none of the considered MA modes allowed us to obtain samples completely consisting of MAX phases for the mixture with x = 0.5. The maximal amount of the Ti_3AlC_2 phase was 55%. In addition, TiC and chromium aluminides are always present the samples. A similar situation is also observed for the mixture with x = 1. The $(Cr,Ti)_3AlC_2$ content does not exceed 50%. It is possible that the phase composition is close to the equilibrium composition for these mixture compositions.

Analogously with [41], properties of synthesized compact products obtained from mechanically activated and nonactivated mixtures were investigated. The materials with the maximal content of the MAX phase are of greatest interest because the properties of the bulk materials with a characteristic laminate structure have been insufficiently studied. It is evident from Table 4 that studied characteristics depend strongly on the phase composition. If a single-phase material, for example, Cr_2AlC (x = 2), is obtained by the synthesis, then characteristics (density, strength, elasticity modulus, hardness, and heat resistance (Fig. 6)) have close values. On the contrary, if phase compositions of samples differ, the difference in properties can be considerable at the same mixture parameter.

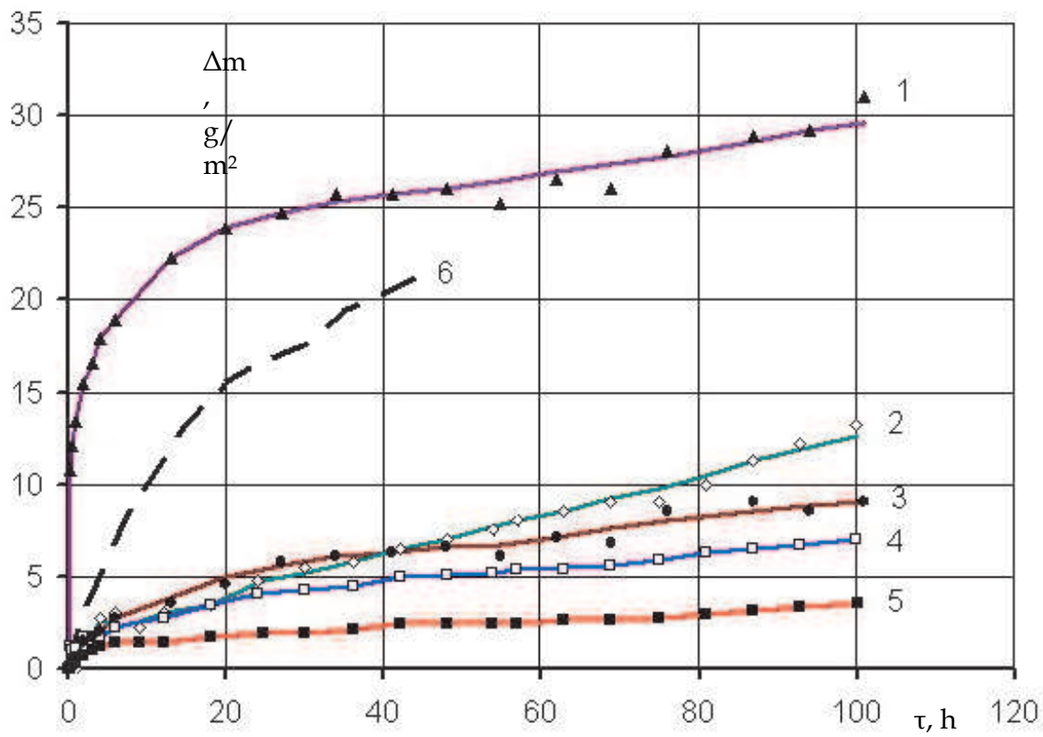

Fig. 6. Time dependence of the variation in the weight of the $Ti_{2-x}Cr_xAlC$ samples at T = 1273 K. (1) x = 0 (NA), (2) 1.0 (NA), (3) 1.5 (NA), (4) 2.0 (NA), (5) 2.0 (MA1), and (6) 83%TiC–17%Cr [48].

Materials with x = 2.0 and 1.5 possess a rather high strength at a large elasticity modulus. Low strength characteristics are mentioned for alloys with a high TiC content. The elasticity modulus was determined from the measurement data of the strength by the three-point

bending method. These results correlate well with the data [38]. The most important service characteristic of this construction ceramic is high-temperature oxidation resistance. Investigations in [41] were carried out at T = 1023 K. Our tests at T = 1273 K developed them. Their results are shown in Fig. 6.

It is seen from curves in Fig. 6 that an increase in the chromium concentration is favorable to a decrease in the weight increment of samples and their oxidation rate and, consequently, to an increase in their heat resistance. The titanium-free Cr_2AlC sample (at x = 2) possesses the highest high-temperature oxidation resistance (Fig. 6, curve 4). When investigating the materials obtained from the activated charge, it was established that their heat resistance is in general somewhat higher than that of materials not subjected to MA and alloys with a high chromium content are better in this respect (Fig. 6, curve 5).

The material synthesized from the MA charge with the mixture parameter x = 1.5 and containing 69 % of Cr_2AlC, 16.6 % TiC, and 14.4 % Cr_4Al_9 has a rather high heat resistance (at T = 1273 K and τ = 100 h, $\Delta m = 7.5$ g/m^2 was obtained). Almost the same weight increment ($\Delta m = 9.1$ g/m^2) was observed for the sample made from the nonactivated mixture containing 54 % Cr_2AlC, 19 % TiC, 22 % Cr_2Al, and 5 % Cr_7C_3.

For synthesis products with x = 1 obtained from the MA mixture, in which the main phases are TiC (43%) and $(Cr,Ti)_3AlC_2$ (45%), the weight increment for the same temperature and time is 6.6 g/m^2, while for samples with the same mixture parameter made from the nonactivated mixture containing 66 % TiC, 8 % Cr_2AlC, and 26 % of chromium aluminides, the increment is 13.3 g/m^2. The increased level of heat-resistance with the use of the MA mixture is explained by the higher concentration of the Cr_2AlC phase in products.

The heat resistance of samples made from the mixture with x = 0.5 (NA and MA) under the mentioned test conditions is 20–25 g/m^2.

The largest weight increment (32 g/m^2) at T = 1273 K and τ = 100 h was mentioned for the material containing no chromium, which can be also caused by the relatively high residual porosity of synthesis products. At the initial stage of tests, an abrupt jump in the oxidation rate associated with the formation of oxide films was observed. This is also valid for samples synthesized from the activated mixture, the weight increment of which for 100 h holding at 1000°C was 27–37 g/m^2. The worst characteristics were obtained for materials containing the largest amount of the Ti_2AlC phase. This result is caused by the fact that, according to the data of differential scanning calorimetry (DSC), the endotherm associated with the decomposition or reconstruction of the Ti_2AlC phase into the Ti_3AlC_2 phase is observed in heating curves at T = 1524–1557 K. This is confirmed by the results of an X-ray structural analysis of the samples after annealing at T = 1473 and 1573 K. In the first case, the amount of the Ti_2AlC phase abruptly decreases from 73 to 16 % and the TiC and $TiAl_2$ contents simultaneously drop to zero, while the amount of the Ti_3AlC_2 phase increases from 16 to 84 %. After the second annealing (1573 K), TiC appears in the samples again in the amount of 45 %, while the Ti_3AlC_2 content decreases to 55 %; the Ti_2AlC phase is unobservable. The second peak in the heating curves at T = 1720–1750 K is apparently associated with the transformation of the Ti_3AlC_2 phase.

For the obtained experimental data on heat resistance, we selected the regression equations (Table 5), which indicated that, for the alloys of the $Ti_{2-x}Cr_xAlC$ system, the growth rate of the oxide film is limited by the diffusion of oxygen. It is described by the equation $\Delta m/S = K\tau^{1/n}$, where Δm is the difference between the current and initial weights of the sample, K and n are the constant coefficients, and τ is the holding time.

X	Mixture preparation	Regression equation
0	NA	$\Delta m / S = 1{,}40\ \tau^{0{,}161}$
0,5	NA	$\Delta m / S = 0{,}517\ \tau^{0{,}687}$
1	NA	$\Delta m / S = 1{,}14\ \tau^{0{,}453}$
2	NA	$\Delta m / S = 1{,}17\ \tau^{0{,}453}$
2	MA	$\Delta m / S = 0{,}517\ \tau^{0{,}401}$

Table 5. Regression equations of the oxidation kinetics of the alloys at T = 1273 K in air

When evaluating the data on the heat resistance of the Cr–Ti–Al–C alloys, we can see that values of this characteristic for them are higher than for simple carbides TiC and Cr_3C_2 and the TiC–17%Cr alloy. The only exclusion is the materials based on the Ti_2AlC and Ti_3AlC_2 phases.
Thus, composite materials in the Ti–Cr–Al–C system, which belong to the class of oxygen-free compounds with a layered structure, possess high heat-resistance and satisfactory mechanical characteristics, which allows us to consider this construction ceramics promising not only as the targets for the magnetron sputtering of heat-resistant, corrosion-resistant, and tribological nanostructured coatings, but also for the fabrication of high-temperature units of constructions operating under extreme exploitation conditions.

3. Borides based ceramic in systems Cr-B and Ti-Cr-B

Borides of transition metals are of special interest in connection with their unique mechanical, thermal, electrical, and magnetic properties. Their use in products of the chemical industry and in the production of abrasives, protective coatings, wear-resistant materials, and construction ceramics is widely known [8, 48–55].
In this section, we consider obtaining ceramic materials based on chromium and titanium borides by SHS pressing [8] from the mixtures, which is preliminarily mechanically activated. The application of MA allows us to perform SHS in low-exothermic systems such as Mo–B and Cr–B [46, 56, 57]. The role of the MA charge manifests itself in a simultaneous increase in the absolute value of heat release and the rate of heat release in the combustion reaction, which exert a positive effect on the thermodynamics and kinetics of the process.
For the studies, we selected a stoichiometric mixture of chromium and boron powders with the weight (in %) component ratio Cr : B = 70.6 : 29.4 calculated for the formation of the CrB_2 compound. The Ti–B–Cr mixtures were formed at a constant ratio Ti/B = 6.14. The composition of the samples under study is presented in Table 6.

Sample	Composition, wt. %		
	Cr	Ti	B
1	70,6	-	29,4
2	30,0	60,2	9,8
3	40,0	51,6	8,4

Table 6. Composition of the green mixtures

Procedures for preparing the samples, carrying out MA, and evaluating the properties of the powder mixtures before and after MA, as well as for determining the SHS parameters and the phase and structure formation in the combustion wave, are presented in [46, 56].
The experimental dependence of the specific heat release (Q) during the chemical reaction on the MA time is presented in Fig. 7. It is evident that the interaction is characterized by a low Q level.

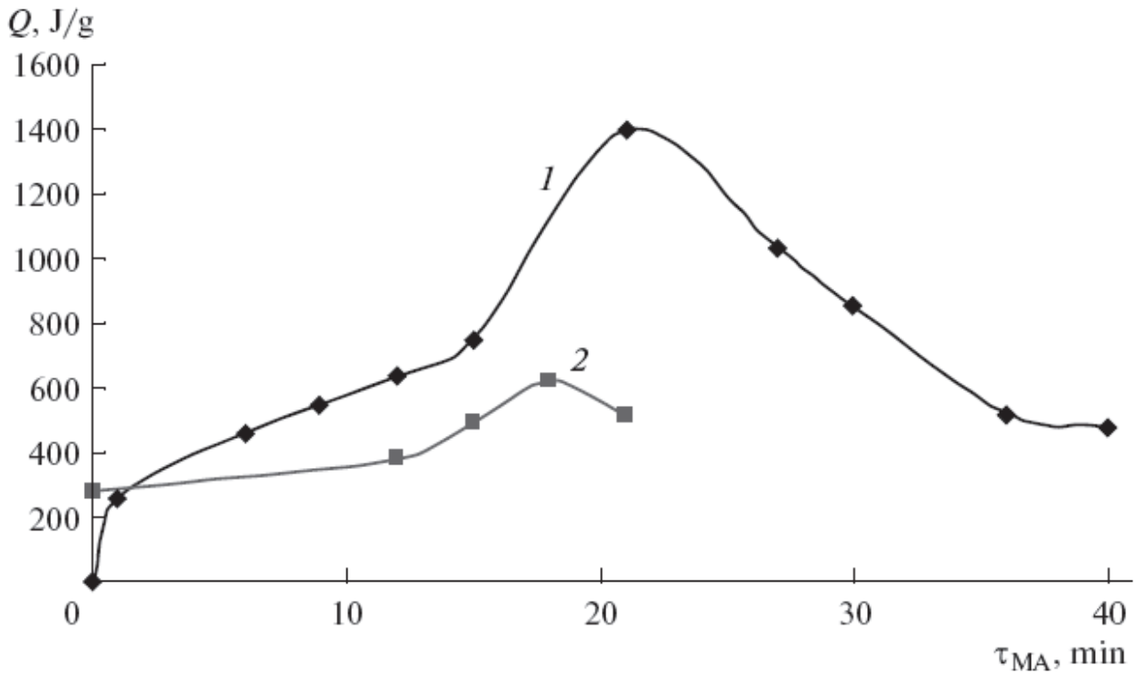

Fig. 7. Effect of mechanical activation duration on the specific heat release. (1) Cr–29.4% B and (2) Ti–40% Cr–8.4% B.

We failed to perform the SHS reaction in calorimeter conditions in the nonactivated Cr–B mixture. Due to the incomplete transformation, the amount of heat released during the combustion was smaller than expected. For example, for weak MA (τ_{MA} = 1 min), the value of Q was 0.3 kJ/g. For comparison, at τ_{MA} = 21 min, Q = 1.4 kJ/g. According to the data of an X-ray phase analysis, intermediate reaction products, lower borides CrB and Cr_3B_4 with lower heats of formation, are present in the combustion products of the Cr–B mixture. A similar pattern was also observed for the Ti–Cr–Br mixtures, where titanium boride TiB and unreacted titanium and chromium are added to lower chromium borides.
Thus, the obtained absolute value of reaction heat turned out to be lower; however, this does not prevent us from following the variation in Q depending on the MA time. As τ_{MA} increases, the amount of released heat increases. This is probably associated with the increase in the transformation depth in the combustion reaction due to the accumulation of macro- and microdefects in starting powders, which leads to an increase in the internal energy of the system, and with the decrease in the heterogeneity scale. The development of the thermal peak in the Cr–29.4% B mixture continues to τ_{MA} = 21 min, while it continues

to τ_{MA} = 18 min in the mixture Ti–40% Cr–8.4% B. Further activation leads to a decrease in the heat release, which is caused by the beginning of mechanochemical reactions of formation of chromium borides during MA. Thus, to obtain the largest Q, the optimal MA time was determined. For the Cr–29.4% B charge, it equals 21 min; for the Ti– 40% Cr–8.4% B mixture, it equals 18 min.

During mechanical treatment, the strain on energy of particles is composed of the energy of subgrain boundaries formed from mosaic blocks, the energy of the new surface formed due to the destruction of the particles, and the elastic deformation energy. In turn, the elastic deformation energy in the crystal depends on the energy of dislocations and vacancies. Each dislocation, possessing a definite energy reserve and being its accumulator in the crystal, is a sublocal limiting distortion of the crystal lattice. The introduction of dislocations into the crystal leads to an increase in its energy, and, as the number of uniformly distributed dislocations increases, the average absorbed energy in the working volume increases [58–62].

The optimal state of the structure of the reagents before SHS corresponds to the definite dislocation structure of the metal and reaction surface of the mixture. To evaluate the effect of MA on the structural state of starting reagents, we analyzed the influence of the treatment time on the structure of the chromium powder. We calculated the size of coherent scattering regions (CSR) according to the broadening X-ray lines. Physical broadening was evaluated by the procedure [63–65]. The results of this investigation are given in Table 7.

τ_{MA}, min	CSR size, nm		Microdeformation, %	
	Cr-29,4%B	Ti-40%Cr-8,4%B	Cr-29,4%B	Ti-40%Cr-8,4%B
1	130,9	-	0.14	-
12	73,1	41,7	0,18	0,150
15	51,6	40,8	0,19	0,211
18	25,6	31,5	0,23	0,267
21	16,0±2	25,9±3	0.27±0,01	0,343±0,05

Table 7. CSR size and microdeformation of the Cr lattice after MA

As the MA time increases, the CSR size decreases, while the microdeformation magnitude increases, which confirms the assumption that the stored energy increases. It should be noted that a decrease in the CSR size in the Cr–29.4%B mixture occurs by an order of magnitude, while the microdeformation increases by a factor of approximately 2. It is evident from the scanning electron microscopy data (Fig. 8) that the mixture initially consists of chromium particles 5–40 μm in size and fine-crystalline boron with the particles of <1 μm. As the MA duration increases, chromium intensely disintegrates and the maximal particle size does not exceed 5 μm, while their spread in regards to size considerably decreases due to the uniform stirring and redistribution of boron over the surface. This leads to an increase in the reaction surface and to a decrease in the kinetic obstacles during the SHS reaction.

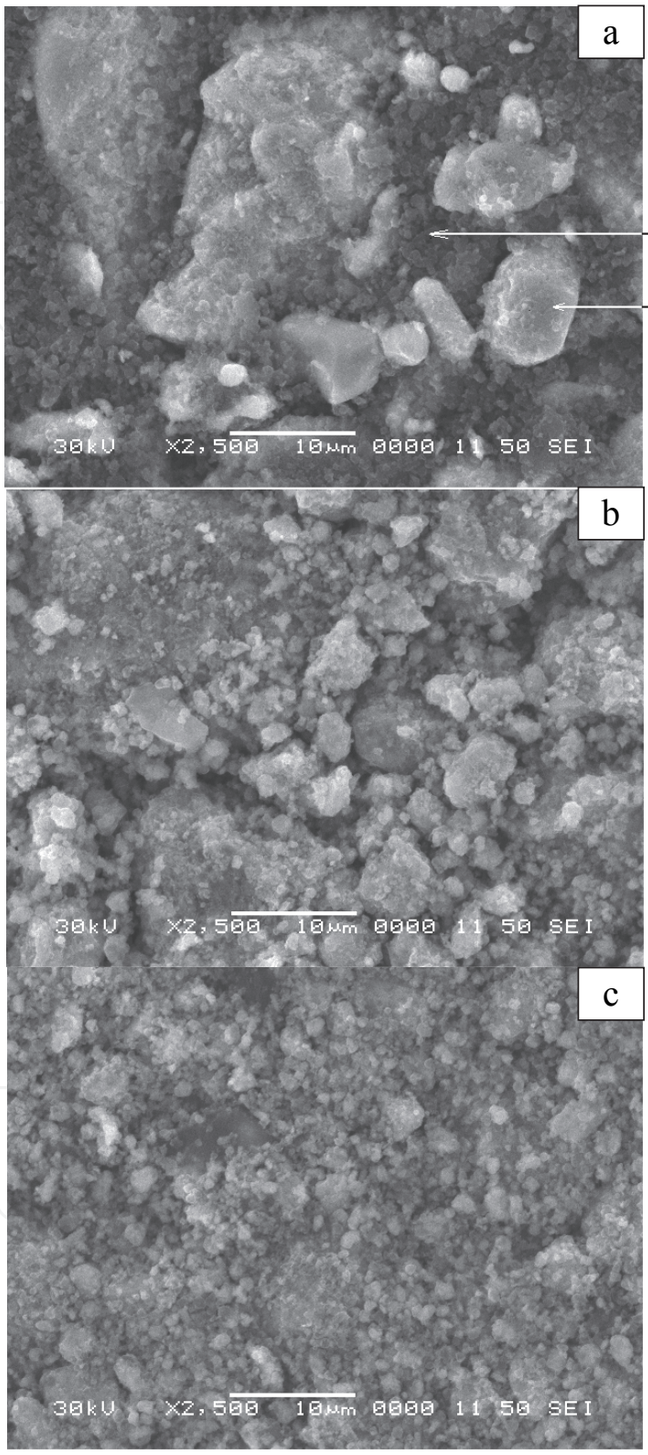

Fig. 8. Morphology of the Cr–29.4% B mixture after MA. τ_{MA}: (a) 1, (b) 21, and (c) 40 min.

During MA, the specific surface of the mixture increases due to the disintegration of powder particles, the formation of cracks, and the accumulation of microstructural and surface

defects. With the MA time longer than a certain critical value (21 min for Cr–B and 18 min for Ti–Cr–B), borides of reagents appear in the mixture; their composition cannot be determined qualitatively by local electron probe microspectral analysis because of the small particle size and difficulties associated with the low atomic number of boron.

The changes that happened in the mixture structure due to MA exert an essential influence on SHS parameters such as the character of propagation of the combustion wave and the combustion temperature and rate. Figure 9 shows the video frames of combustion of the activated Cr–B mixture. The combustion wave is spread along the axis sample downwards. The combustion source (frame 2), like the "spin", moves in the plane perpendicular to the propagation direction of the combustion wave (frame 3). After the source passes through the sample plane (frame 4), the combustion passes to the following layer (frame 5). The pattern is periodic and repeats itself through equal time intervals (0.16 s). This indicates that the character of combustion of the activated sample is time-dependent near the stability limit.

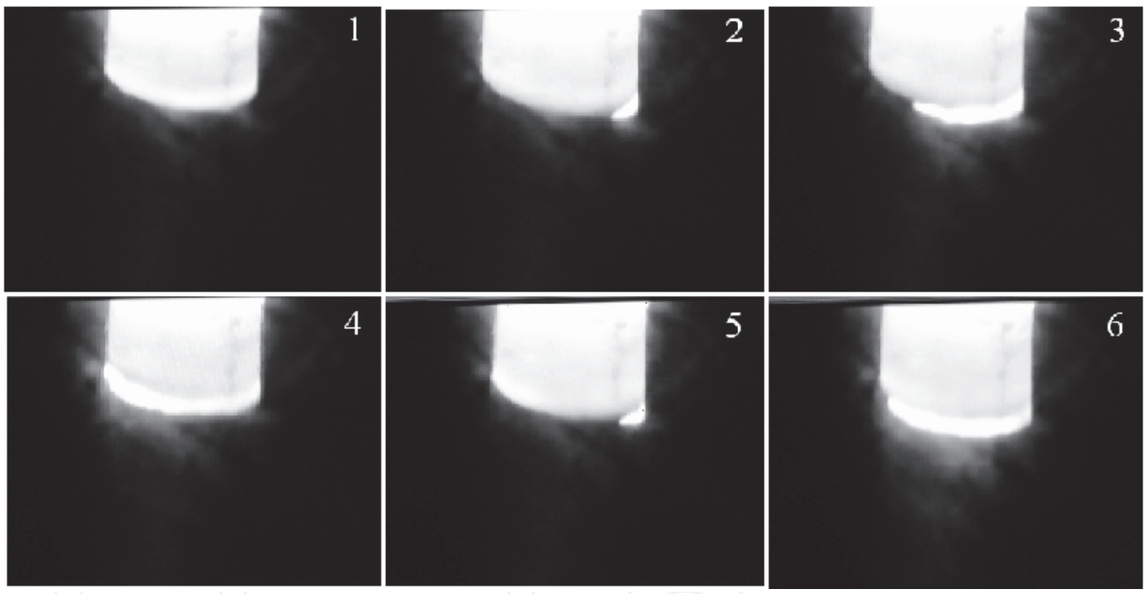

Fig. 9. Frame-by-frame video filming of the combustion of the Cr–B mixture after MA. τ_{MA} = 21 min, T_0 = 293 K, and V_{film} = 25 frame/s.

An investigation of samples macrostructure showed the presence of stratification in products obtained from the Cr–B mixture activated for 21 min. The periodic character of transversal cracks repeats the motion of the combustion front.

On the contrary, the structure of the combusted sample of the slightly activated Cr–B mixture is uniform and contains no visible transversal stratification corresponding to the character of propagation of the combustion front.

The result of a measurement of the combustion rate as a function of the initial temperature is shown in Fig. 10. It is possible to implement SHS in MA mixtures at T_0 = 300 K; in the slightly activated (τ_{MA} = 1 min) Cr–29.4% B mixture, this is possible only at T_0 = 525 K; and in the nonactivated Ti–30% Cr–9.8% B and Ti–40% Cr–8.4% B mixtures, it is possible only at T_0 = 523 and 653 K, respectively. For all compositions, the linear dependence of U_c from T_0 is

observed. In the MA Cr–B mixtures, the formation of chromium boride occurs with a considerably higher rate and depends more strongly on the initial temperature than in the Ti–Cr–B system. For all three MA compositions at T_0 > 530–540 K, the combustion sources are formed throughout the sample volume (combustion is similar to heat burst) and their motion is directed chaotically. The combustion rate cannot be determined under these conditions, because we determined it as the distance passed by the combustion wave along the sample axis for a certain time interval.

It is evident from Fig. 10 that, for activated Cr–B and Ti–Cr–B mixtures, the combustion rate is higher at the same initial temperature than nonactivated or slightly activated mixtures. For example, for the Cr–29.8% B composition at T_0 = 525 K, after activation for 1 min, U_c = 1.8 mm/s, while it is 8.7 mm/s for τ_{MA} = 21 min. Thus, we observe the substantial influence of MA on the combustion process. This effect corresponds to the published data [44–46, 57–60, 62] on the positive influence of MA on combustion kinetics and mechanism for different SHS systems.

One interesting feature of Cr–B and Ti–Cr–B materials under study which is not inherent to other previously studied systems is the fact that the combustion temperature (T_c) depends very weakly on T_0 in a certain range of T_0. This effect manifests itself for the Cr–B mixture both after strong and weak activation (Fig. 10b), while it is observed only after strong activation for the Ti–Cr–B system.

It is established experimentally that, for the slightly activated Cr–B mixture, T_c = 1800–2200 K, which is close to the adiabatic temperature (1900–2200 K) calculated using the THERMO program, while T_c is noticeably lower for the strongly activated mixture (τ_{MA} = 21 min) and equals ~1500 K, despite a considerable increase in the combustion rate.

It should be noted that the T_0-dependences of T_c shown in Fig. 10b for the activated and nonactivated Ti–Cr–B mixtures differ qualitatively. In MA mixtures in the range of T_0 from room temperature to 450 K, an increase in the initial temperature either does not exert the combustion temperature in practice (sample 3) or it affects it insignificantly (sample 2). This character of curves 2 and 3 is usually attributed to the processes with heat absorption. As was mentioned above, the combustion rate of the activated mixtures at T_0 ~ 530–540 K increases abruptly, which leads to the spread of the analyzed material due to the abrupt release of the gases absorbed during MA and the loss of contact between the sample and thermocouple. Therefore, we failed to measure the combustion temperature at T_0 > 530–540 K for the activated Ti–Cr–B samples. In nonactivated Ti–Cr–B mixtures, a linear dependence is observed between the combustion temperature and the heating temperature of the mixture.

To clarify the mechanism of combustion and structure formation, we quenched the sample in a copper wedge. Figure 11 shows the microstructure of the stopped combustion front (SCF). The quenched combustion zone is arranged near the line 1–1; combustion products that formed after the SHS reaction is stopped are above this line, and the heating zone and the starting reaction mixture are below it.

During a detailed analysis of the phase composition in the combustion zone and behind the combustion front in the region of the formed products, we established the following. In the combustion zone, we can distinguish the regions of different coloration, which is caused by different chemical compositions. Light regions (Fig. 12a, point 3a) are enriched with chromium, while gray regions (points 2a, 4a) are enriched with titanium (Table 8). Unreacted oxygen-containing starting components are present in separate dark segments (point 1a).

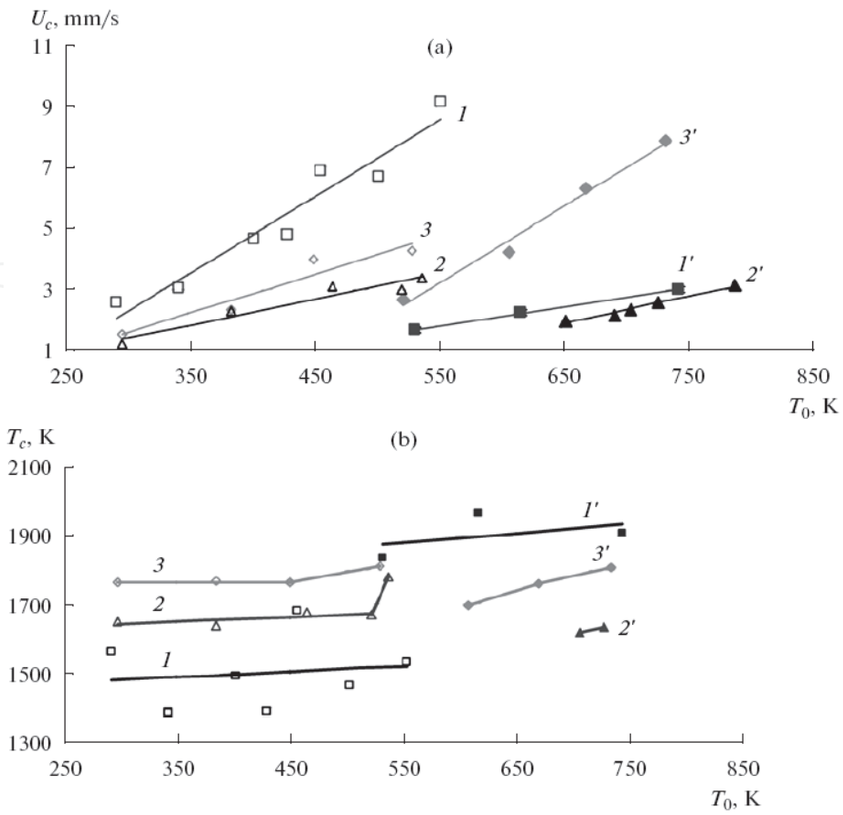

Fig. 10. Dependences of the combustion (a) rate and (b) temperature on the initial temperature of the process for the Cr–B and Ti–Cr–B green mixtures obtained for various MA times. (1, 1') Cr–29.4% B, (2, 2 ') Ti–40% Cr–B, and (3, 3 ') Ti–30% Cr–B. (1–3) Strongly activated (τ_{MA} = 21 min (1) and 18 min (2, 3); (1') slightly activated (τ_{MA} = 1 min) and (2 ', 3 ') nonactivated.

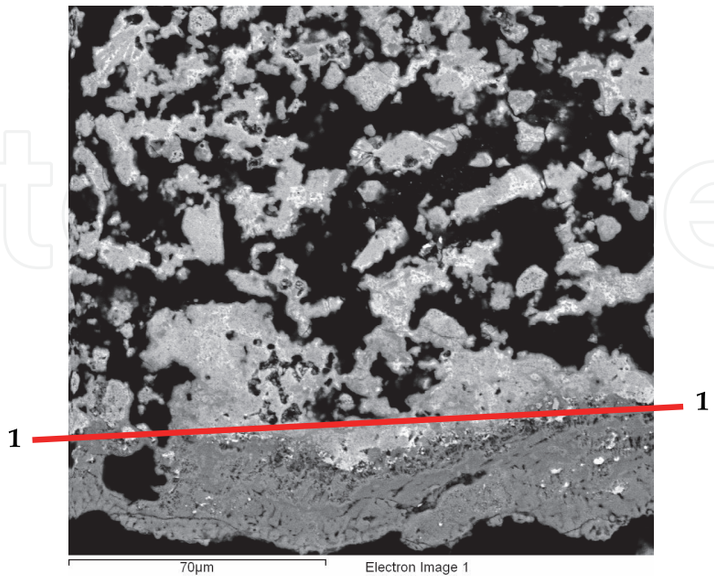

Fig. 11. Quenched combustion front of the Ti–30%Cr–B MA sample.

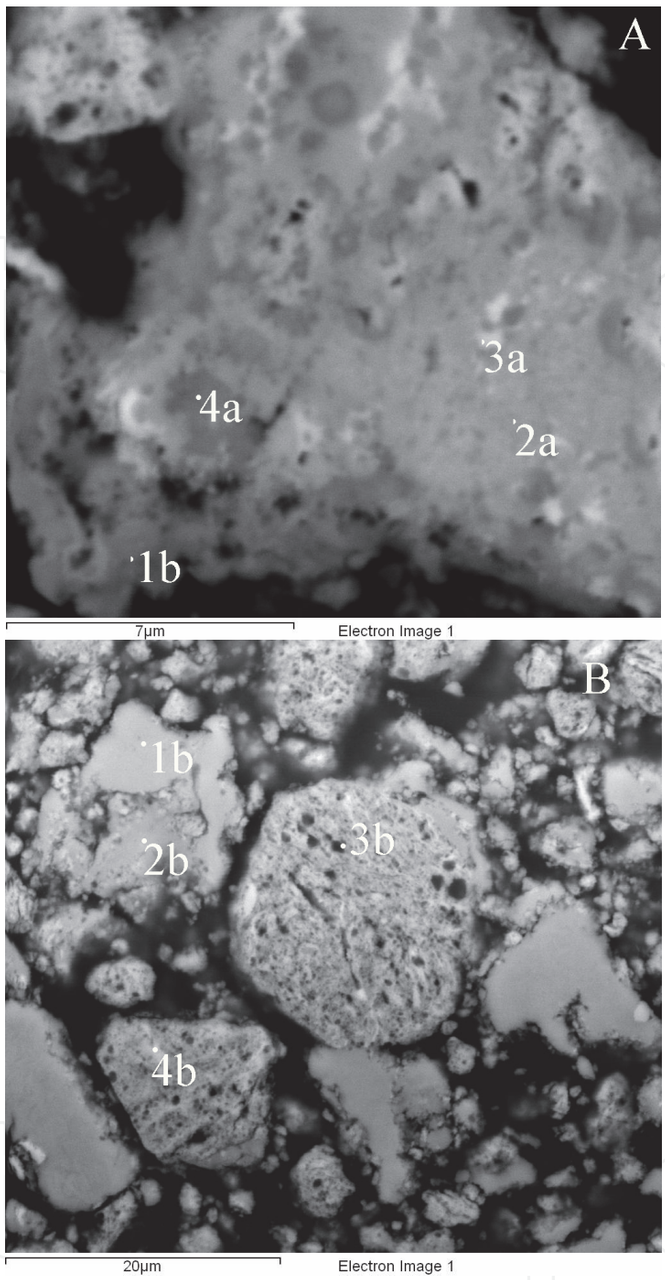

Fig. 12. Stopped combustion front (Fig. 11, the region above line 1–1) of the Ti–Cr–B mixtures. Magnification (a) 5000× and (b) 1500×.

Behind the combustion front, we can also distinguish the regions differing both in color and form. Similarly to those described above, light regions (point 3b) are enriched with chromium, while light gray and dark gray regions are enriched with titanium. Taking into account morphological features of these regions (acicularity or roundness), we can assume their phase composition. The regions with a characteristic needle shape contain titanium and chromium borides, while rounded irregular shapes are characteristic of the starting reagents or a solid solution based on metals. The reagents start to interact at the particle

surfaces. For example, point 1b in Fig. 12b belongs to titanium, while the interaction between Ti, Cr, and B already passed in point 2b. Light needlelike formations correspond to titanium or chromium borides. However, we should note that it is very hard to exactly determine the formation sequence of the phases because of their variety and the similar elemental composition of the intermediate phases. Table 8 shows elemental composition of the Ti–Cr–B sample in each point.

Point № in Fig. 12	B	O	Ti	Cr
1a	16.16	20.58	57.58	5.68
2a	15.42	-	72.62	11.45
3a	22.02	-	65.20	12.42
4a	11.57	-	82.72	5.55
1b	-	-	99.50	0.50
2b	17.89	-	80.64	1.37
3b	56.00	3.66	10.12	29.26
4b	48.15	3.05	15.15	21.63

Table 8. Elemental composition of the Ti–Cr–B sample, wt %

An analysis of possible reactions in the combustion waves of the Ti–Cr–B and Cr–B mixtures under consideration is presented below. Analogously to the Mo–B system [57], the following reactions proceed in the heating zone:

$$B_2O_3(sol) + B \rightarrow 3/2B_2O_2(g) - Q, \quad (4)$$

$$Me + 2B \rightarrow MeB_2 + Q. \quad (5)$$

The solid-phase interaction between chromium and boron in the heating zone is inlikely because of the relatively low diffusion atomic mobility at these temperatures. However, the reversible gas-transport reaction (4) of the formation of volatile boron suboxide occurs on the reagent surface at T = 1100–1250 K. In the combustion wave, it is preceded by the melting of boron oxide B_2O_3 at T = 723 K [57]. Gaseous suboxide is chemisorbed on the surface of the chromium and titanium particles with the formation of the most thermodynamically favorable boride phases, for example, by the reactions:

$$3B_2O_2(g) + 3Ti \rightarrow 2B_2O_3(liq) + TiB_2 + 2Ti + Q \rightarrow 2B_2O_3(liq) + 2TiB + Ti, \quad (6)$$

$$B_2O_2(g) + Cr \rightarrow B_2O_3(liq) + Cr_yB_z + Cr + Q. \quad (7)$$

Thus, the saturation of particles of the reagent metal with boron goes from the surface to the center. Then the product formed in Ti–Cr–B system after combustion zone interact with formation of the ternary boride compounds:

$$TiB + Cr_yB_z \rightarrow CrTi_2B_2 \text{ and } TiB + Cr_yB_z \rightarrow Cr_4Ti_9B \quad (8)$$

as well as the solid solutions and Ti–Cr compounds.

In parallel to mentioned reactions, the endothermic reaction occurs in the heating zone (in front of the combustion front):

$$B_2O_3(sol) + B \rightarrow 3/2B_2O_2(g) - Q, \quad (9)$$

An analysis by oxygen for the Cr–B mixture showed that its fraction is 0.4% in the starting powder chromium, while its fraction is 3.7% in the starting boron. The recalculation for the specified composition of the mixture shows that chromium introduces 0.28% oxygen, boron introduces 1.09% oxygen, and its total content is 1.37%. After MA for 1 min, this characteristic of the charge increases to 2.6% (almost by a factor of 2), and, after 21 min MA, it increases to 3.3%. This excess oxygen increases the concentration of boron and chromium oxides. If we decompose the total amount of oxygen for the mixture reagents, we obtain that, in the case τ_{MA} = 21 min, its fraction in chromium is 0.66%, while its fraction in boron is 2.64%, which corresponds to 3.83% B_2O_3 in the mixture. Thus, boron is the main oxygen carrier in the mixture; 80% of oxygen in the mixture composition is associated with boron, and only 20% is associated with chromium. Such a distribution shows that the contribution chromium oxide to the combustion mechanism and kinetics is not determinative. As the oxygen content in the mixture increases due to MA, the role of the gas-transport boron transfer to the metal surface increases and the reaction diffusion becomes the limiting stage of the interaction between the metal and boron.

We carried out a thermogravimetrical analysis of boron and chromium powders at T = 300–1273 K, as well as the green mixtures mechanically activated for 1 and 21 min. It was established that, in the mentioned temperature range, chromium undergoes no substantial phase transformations accompanied by thermal peaks and a change in weight. The endothermic transformation with an energy of 2.0 kJ/g proceeds in the boron powder at T = 1020–1250 K. Endothermic peaks are also observed for the MA charges. In the case of τ_{MA} = 1 min, this peak is located at T = 1020–1230 K and the thermal absorption is 0.18 kJ/g; at τ_{MA}, this peak is located at T = 900–1020 K and the thermal absorption is 0.9 kJ/g.

The results of qualitative and quantitative X-ray phase analyses of the composition of the synthesized samples showed that, in the case of a strongly activated Cr–29.4% B mixture, as T_0 in the combustion products increases, the fraction of higher chromium borides increases as the amount of boride phases decreases. This occurs during the transition $CrB \rightarrow Cr_3B_4 \rightarrow CrB_2$ by the solid-phase reactive diffusion mechanism; stage I passes almost completely due to the large amount of accumulated energy. However, subsequent stage II has no time to be completed. The product consists of two-phase (CrB_2 and Cr_3B_4) with a small amount of fine pores.

As a result of an X-ray phase analysis of the SHS products in the Ti–Cr–B system under study, previously unknown Cr_4Ti_9B and Ti_2CrB_2 phases were found. In addition, these samples contained TiB and $TiCr_2$ phases. Due to the preliminary MA of the Ti–30% Cr–9.8% B mixture, we succeeded in completely eliminating the $TiCr_2$ intermetallic compound and increasing the content of complex Ti_2CrB_2 boride.

According to the result of our investigations, we synthesized large-scale samples 125 mm in diameter based on chromium borides of compositions Cr–29.4% B, Ti–30%Cr–9.8%B, and Ti–40%Cr–8.4%B. The addition of titanium into the reaction mixture allowed us to decrease the residual porosity from 6% in the Cr–B compact samples to 2% in the Ti–Cr–B synthesis products, which improved the exploitation properties of target materials.

4. Tantalum containing ceramic targets in system Ti-Ta-C

Tantalum finds a wide application in reconstructive surgery, mainly due to its high strength and hardness combined with excellent plastic characteristics, high chemical stability, and

good biological compatibility. Analogously with other carbides and nitrides of transition metals, TaC and TaN possess high hardness, wear resistance, and corrosion resistance. In [66], the macrokinetic features of the combustion of the mixture with the composition (90% – x)(Ti + 0.5C) + x(Ta + C) + 10% $Ca_3(PO_4)_2$, as well as the structure and properties of the synthesis products were investigated depending on mixture parameter x. During these investigations, the temperature profiles of the combustion wave with two peaks of heat release were detected, which indicates that the chemical reactions are staged, and the combustion proceeds in the detached mode. For example, as the charging parameter increases to x = 45% and the initial temperature of heating increases to T_0 = 420 °C, the two peaks merged. The combustion transformed from the detached mode into the coalescence mode, but an increase in x parameter did not lead to a noticeable variation in the combustion rate.

It is known that, in the Ti–C system, the leading SHS stage is the reactive diffusion of carbon into the titanium melt, while it is the diffusion of carbon into tantalum in the Ta–C system [7, 8, 66–69]. Carbon is transported to the surface of tantalum particles through the gas phase via the circulation of CO and CO_2 by the Buduar–Bell cycle [8].

Upon the addition of a certain amount of the Ta + C mixture into the Ti + 0.5C powder mixture, parallel or sequential chemical reactions of the formation of titanium and tantalum carbides occur in the combustion wave. Taking into account the fact that the combustion mechanisms of the mentioned mixtures are different, we should expect that, depending on the amount of the added Ta + C mixture, the moving force of the combustion is either the dissolution of carbon in the titanium melt (after the formation of the reaction surface via the capillary spread of the melt over carbon) or the solid-phase reactive diffusion of carbon into tantalum. In the latter case, the gas transport of the carbon reagent to the surface of the solid Ta particle and the formation of tantalum carbide proceed according to the following scheme: the interaction of the CO_2 molecule with carbon along with two moles of CO being obtained; the gas transport of 2CO to the surface of the Ta particle; the chemisorption of 2CO on the surface; the two-stage interaction between tantalum and carbon with the initial formation of tantalum semicarbide and then tantalum carbide by the scheme Ta + 2CO → TaC + CO_2; the desorption of the CO_2 molecule from the surface of the formed tantalum carbide layer; the transport of CO_2 to the surface of the carbon particle; and the interaction between CO_2 and carbon with the formation of 2CO, etc [7, 66].

In their conclusions, the authors of [66] used the published data on the mechanisms of combustion and structure formation in the Ta–C and Ti–C binary systems, since the mechanism of the phase formation of the SHS products in the Ti–Ta–C ternary system is practically unknown. In connection with the difficulties in interpreting the obtained results, the authors of [66] additionally investigated SHS in the Ti–Ta–C ternary system [69] without the addition of calcium orthophosphate while varying the charging parameter from the minimal (10%) to maximal (50%) value. In this case, powder materials were used, namely, titanium and carbon of the above-mentioned grades and the tantalum TVCh (TU 95-251-83).

The compositions of the exothermic mixtures were varied according to the condition (90%–x)(Ti+0.5C) + x(Ta+C), where the mixture parameters corresponded to x = 10, 30, and 50% (Table 9).

The procedure of preparing the sample, the investigation methods, and the equipment are described in detail [64, 69]. The experimental dependences of the temperature and combustion rate on the initial temperature for mixtures with various values of x are shown in Fig. 13.

x, wt %	Mixture composition, wt %			Calculated adiabatic combustion temperature, K	Combustion rate, cm/s
	Ti	Ta	C		
10	80,0	9,5	10,5	1988	0,51
30	62,3	28,1	9,6	2132	0,42
50	44,5	46,9	8,6	2329	0,27

Table 9. Mixture compositions and characteristics of the SHS process

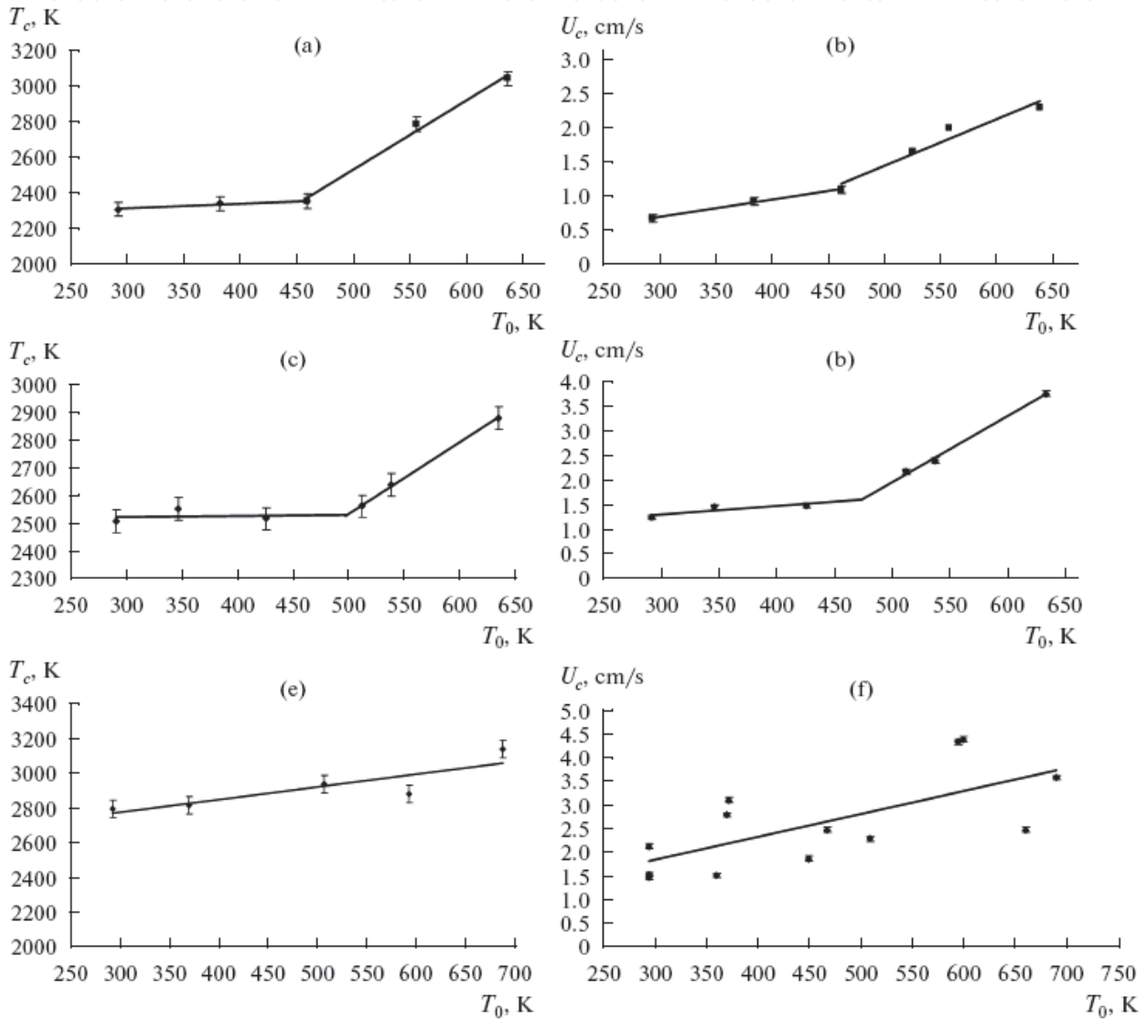

Fig. 13. Dependences of the temperature (a, c, e) and combustion (b, d, f) rate from the initial heating temperature of the mixture at various mixture parameters. x: (a, b) 10, (c, d) 30, and (e, f) 50 wt %.

It is evident from Fig. 13 that in the range of T_0 from room temperature to 450–500 K, the combustion temperature of the under studied mixtures increases linearly. For the compositions with x = 10 and 30%, the combustion rate and temperature abruptly increase at T_0 > 450 K, which indicates the change in the combustion mechanism.

The heating curves of the combustion wave with various charging parameters were analyzed in [66]. It was shown that, at x = 10%, the temperature profile has a complex character, which is associated both with the stage character of the reaction and with microstructural features of the process; namely, the deformation of the medium and the formation of separate hot reaction sources near the thermocouple. In addition, the onset of the reaction is accompanied by an abrupt increase in temperature, which indicates that the first stage of the reaction proceeds rapidly. Then an abrupt drop of T_c follows. Such behavior is typical of cases when the combustion proceeds by the relay race mechanism. Similar results were obtained in [69] when analyzing the profiles of heating curves.

The dependences of T_c and U_c on the initial temperature in the range T0 = 300–700 K for the mixture with x = 50% (Figs. 13e, 13f) are close to linear, which indicates the unique combustion mechanism and that the parallel chemical reactions of the formation of titanium and tantalum carbides proceed in a wide combustion zone. However, with the detailed consideration of the heating curve of combustion (Fig. 14) recorded at various T_0, it is evident that two peaks of heat release with temporal resolution of 0.2 s can be distinguished upon heating to 493 K and above. An analysis of these heating curves confirmed the effect associated with the formation of two peaks established in [66].

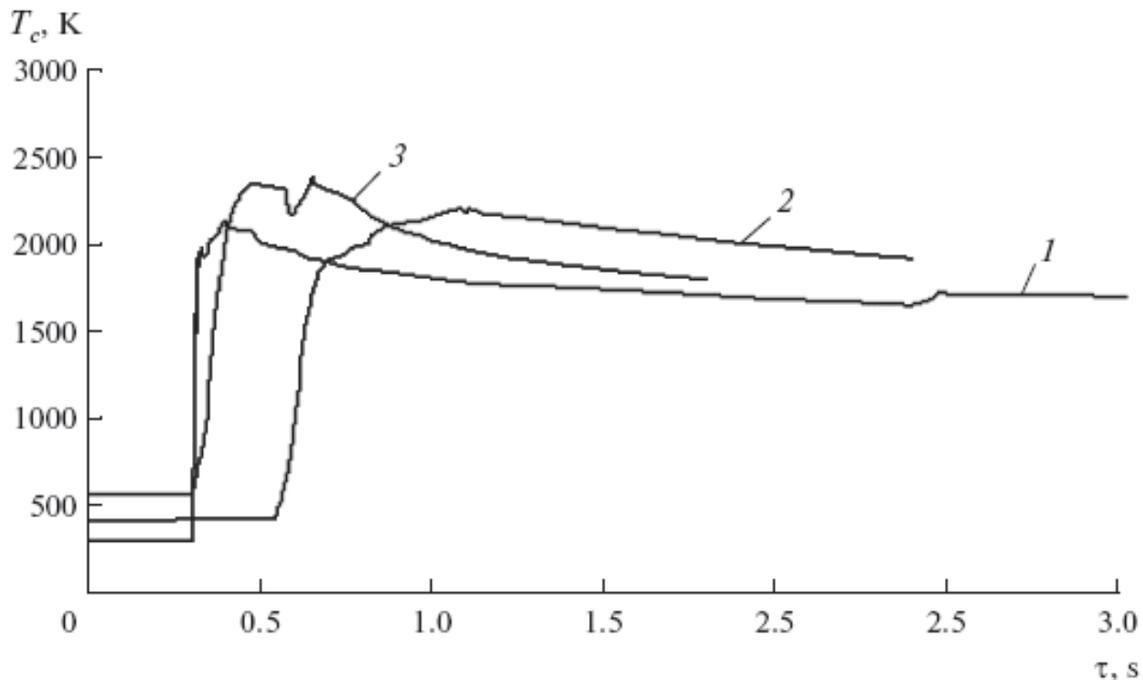

Fig. 14. Temperature profiles for the sample with x = 50%. T_0: (1) 293, (2) 388, and (3) 493 K.

This character of the profile of the combustion wave is possibly associated with the fact that, as T_0 increases, the spatial separation of the chemical reactions proceeding by different mechanisms and having different activation energies takes place. This can be interpreted in the context of the theory of the combustion waves upon two and more parallel or sequential reactions occurring [70–72]. In the mixtures with a low Ta concentration in the combustion front, titanium interacts with carbon through the stage of melting and the capillary spread of titanium over the developed ash surface. In this case, tantalum reacts with carbon in the

afterburning zone. Such combustion mode is usually called the detached mode. As the Ta content increases, the intensity of the second reaction increases, while that of the first reaction (titanium–carbon) substantially drops, and the combustion gradually transforms into the coalescence mode. For the mixture with x = 50%, the contribution of the reaction of the formation of tantalum carbide becomes more noticeable, and, at T_0 > 500 K, the combustion (without a noticeable variation in its average rate) apparently gradually transforms into the detached mode.

It is seen from Fig. 13 that, at T_0 = 300 K, as the mixture parameter increases, the combustion temperature increases from 2250 K at x = 10% to 2600 K at x = 50%, which is in good agreement with the calculated value of the adiabatic temperature of combustion. According to this, due to the higher value of T_c^{ad} of the Ta + C = TaC mixture (2736 K) when compared with the Ti + 0.5C = $TiC_{0.5}$ of the nonstoichiometric composition (2218 K), the integrated combustion temperature of the ternary mixture increases (Table 9).

The presented experimental data on the combustion rate (Fig. 13) illustrate the proportional T_0-dependence of U_c. For each value of x, the combustion rate increases as T_0 increases. It also increases as charging parameter x increases. Based on the available data on average combustion rates of the Ta + C = TaC and Ti + 0.5C = $TiC_{0.5}$ mixtures (0.6 and 2.0 cm/s, respectively [8]), the increase in the combustion rate is explained by the conservation of the leading role that the reaction of titanium carbide formation plays even at the highest tantalum content in the mixture. An increase in x leads to an increase in the carbon concentration in the mixture with respect to titanium. Consequently, by the first stage, more stoichiometric titanium carbide can form. The closer its composition is to stoichiometry, the larger the amount of heat is released, which determines the increase in the combustion rate.

The compositions of the synthesis products and lattice parameters of the obtained complex titanium–tantalum carbide are listed in Table 10.

x, wt %	Mixture composition, wt %	Phase composition of the combustion product	Lattice constant (a), nm
10	Ti- 9,5%Ta-10,5%C	(Ti,Ta)C	A = 0,4304
30	Ti-28,1%Ta-9,6%C	(Ti,Ta)C	A = 0,4316
50	Ti-46,9%Ta -8,6 C	(Ti,Ta)C	A = 0,4331

Table 10. Results of an X-ray phase analysis of the synthesis products depending on the mixture parameter

It is evident that, for all the values of the charging parameter, the product is the (Ti,Ta)C complex carbide. The view of a typical diffraction pattern is invariable for all studied compositions in view of the complete mutual solubility of titanium and tantalum carbides. As the Ta content in the mixture increases, the lattice parameter of carbide increases. The variation in the lattice parameter is close to the calculated one; it completely agrees with the published data [72, 73].

To investigate the dynamics of the phase formation and structure formation of the products of synthesis, experiments on stopping the combustion wave in a copper wedge with the angle at a vertex no larger than 5° with a subsequent electron microscopy investigation and electron probe microstructural analysis of the characteristic segments of the SCF were carried out. This allowed the authors of [69] to show the dynamics of transformations in the

combustion wave of the ternary system under study. The microstructures recorded in different regions of the SCF are shown in Figs. 15 and 16 by the example of a sample with x = 10%. The microstructure of the combustion front is presented in Fig. 15. The heating zone with the initial still unmolten Ti particles 10–80 μm in size (marks 1 and 2 on the light-gray particles) is situated to the left of the visible combustion front. The combustion zone, or the reacting medium after titanium is melted and its capillary is spread over the ash surface, is observed to the right of the combustion front (marks 3 and 4 with the component ratio Ti 90% and C 10%). White Ta particles 40–60 μm in size are also seen (marks 5 and 6).

The primary structure formation, which starts in the combustion zone, can be observed in Fig. 15c. Here, the finest grains of nonstoichiometric titanium carbide are isolated from the supersaturated titanium melt. The primary Ti–C crystals are noticeably smaller than 1 μm. As it goes further from the combustion zone to the zone where the reaction is completed, the Ti–C grains grow to 2–3 μm in size.

It is interesting to follow the regions in which the Ta particles are situated. Particles of the titanium–tantalum solid solution with content up to 6.5% Ti are found near the combustion front. This solid solution was formed due to the dissolution of Ta in the Ti melt and contains almost no carbon. The Ta particles start to react noticeably later, only in the region of where the reaction is completed. Figure 16a shows the reacting Ta particle. The dissolution occurs here, specifically, the diffusion penetration of tantalum (tantalum carbide) into the Ti melt and into the sublattice of nonstoichiometric titanium carbide. In this case, the regions of the diffusion influence of tantalum are more lightly colored.

According to microanalysis data, the composition of white particles corresponds to the initial tantalum powder, and the light-gray regions are enriched with titanium and comprise the agglomeration of titanium carbide grains. However, during a more detailed analysis of the distribution of elements inside these grains (see Fig. 16c), it is seen that the titanium content is higher in the center of the grains, while that of tantalum is higher at their periphery. The formation of a typical ring structure indicates that, initially, titanium carbide grains are formed; their further growth (the secondary structure formation) proceeds due to the dissolution of tantalum or tantalum carbide in them. In this case, the Ta content in the carbide grain depends on the heterogeneity scale. Carbide grains (Ti,Ta)C with an increased Ta content are formed near the places where dissolving Ta particles are arranged (Figs. 16b, 16c). Thus, the structural microinhomogeneity is determined by the size of the Ta particles.

The SCF at x = 30% is also characterized by two structural components, namely, white tantalum particles conserving the shape and sizes and gray regions, which comprise the agglomeration of titanium carbide grains. However, despite the fact that the tantalum content in the mixture is higher, its content in titanium carbide grains is lower than in the sample with x = 10% in this case. This is apparently associated with the fact that the amount of titanium decreases in the reacting system with a large charging parameter and the diffusion transition of tantalum into titanium carbide is retarded. In general, immediately behind the combustion front, the structure consists of two carbides, titanium carbide and tantalum carbide, and a small amount of complex carbide (Fig. 17a, Table 11). Complex carbide is formed due to the complete mutual solubility of titanium and tantalum carbides. Then carbide grains coalesce in the afterburning region due to the fact that they grow as Ti and Ta are dissolved in TiC.

A similar pattern is observed during an investigation of the SCF of the mixture with the largest mixture parameter x = 50% [69]. An expressed structural separation in regards to the

composition of individual regions is noted (Fig. 17b, Table 12). In particular, a larger amount of the regions that comprise either tantalum carbide or titanium carbide is formed. However, the Ta content in the (Ti,Ta)C carbide increases compared with x = 30%.

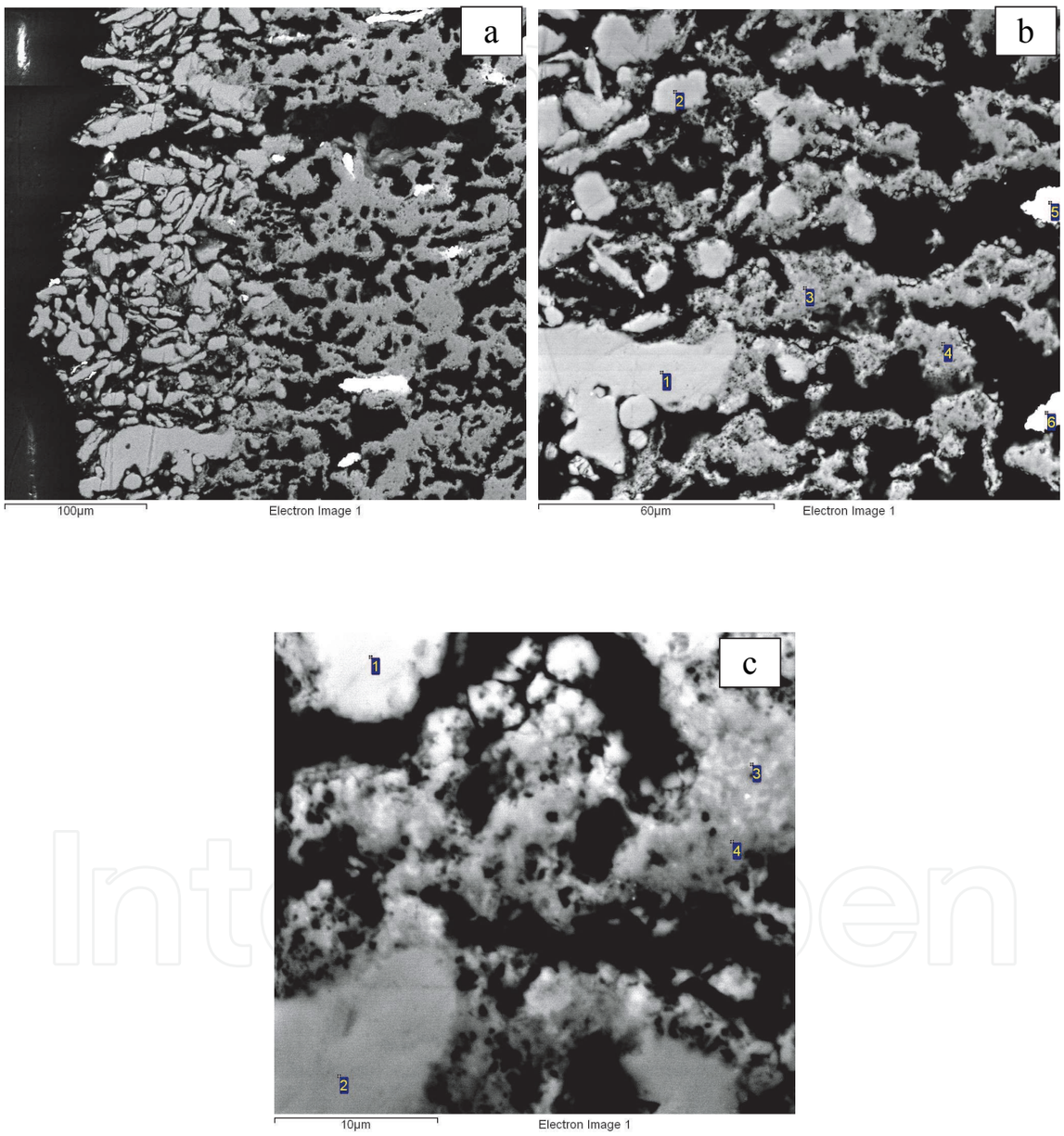

Fig. 15. SCF microstructure at x = 10% near the combustion front. (1, 2) Starting Ti particles in the heating region, and (3, 4) the reacting medium in the combustion zone (after melting Ti and its capillary spread over the surface with the component ratio Ti 90%, C 10%).

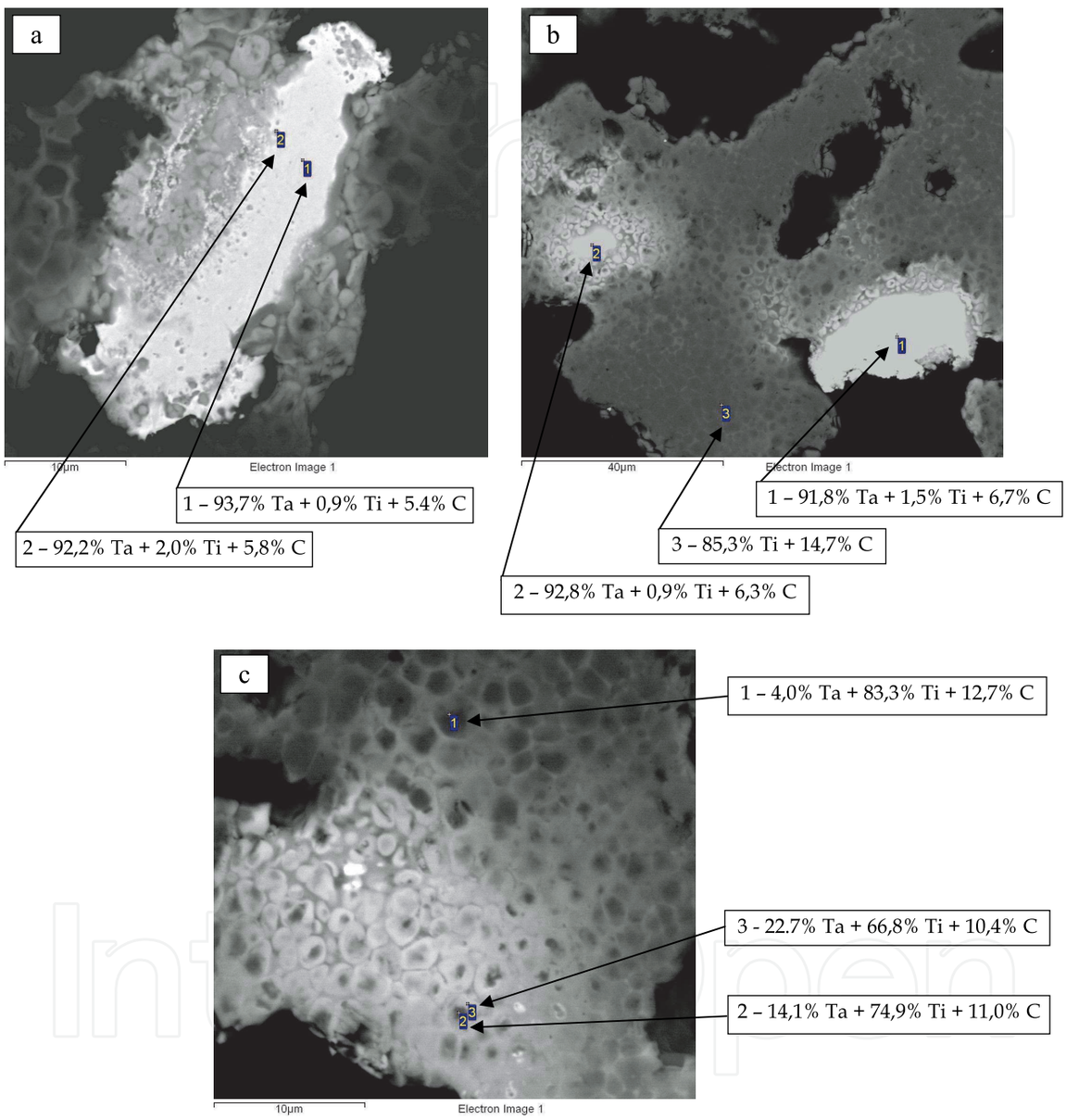

Fig. 16. SCF microstructure at x = 10% in the zone of completing the reaction. (a, b) Reacting Ta particles and (c) formed grains of the (Ti,Ta)C complex carbide, or secondary structure formation.

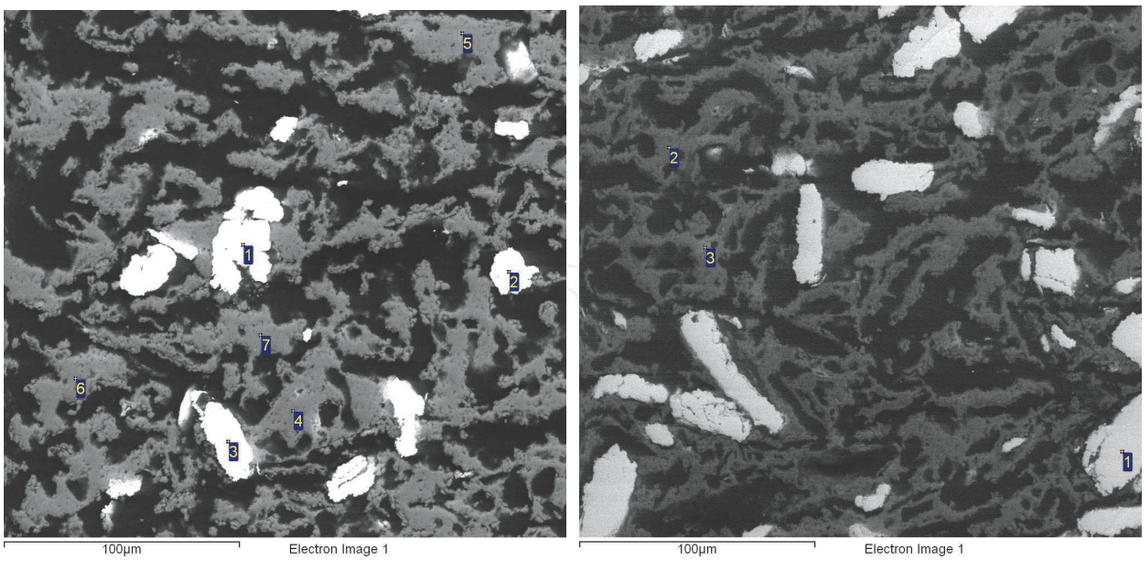

Fig. 17. SCF microstructure at x = 30% (a) and x = 50 % (b).

Point №	Content, wt %		
	C	Ti	Ta
1	4,03	0,00	95,97
2	3,15	0,76	96,09
3	5,07	0,00	94,93
4	15,19	84,81	0,00
5	14,91	84,00	1,09
6	14,43	84,15	1,42
7	13,42	86,58	0,00

Table 11. Results of a microanalysis of various regions at x = 30% in Fig. 17a

Point №	Content, wt %		
	C	Ti	Ta
1	-	-	100,00
2	23,18	76,82	
3	27,12	66,22	6,66

Table 12. Results of a microanalysis of various regions at x = 50 % in Fig. 17b

It follows from an analysis of the microstructures of the products of the synthesis obtained by the technology of the forced SHS pressing that the average size of the carbide grain (Ti,Ta)C decreases from 8 to 4 µm as x increases [69]. This fact can be interpreted only from the viewpoint of the stoichiometry of the formed carbide grains. As x increases, the degree of imperfection of titanium carbide grains by carbon decreases; consequently, the diffusion

mobility of carbon atoms in a more stoichiometric carbide lattice increases [74]. The crystallization and recrystallization of the carbide grains through the liquid phase is retarded. A decrease in the amount of the melt is also the cause of a decrease in the growth rate of the carbide grain.

Obtained materials were tested for high-temperature oxidation resistance at T = 1073 K in air (Fig. 18).

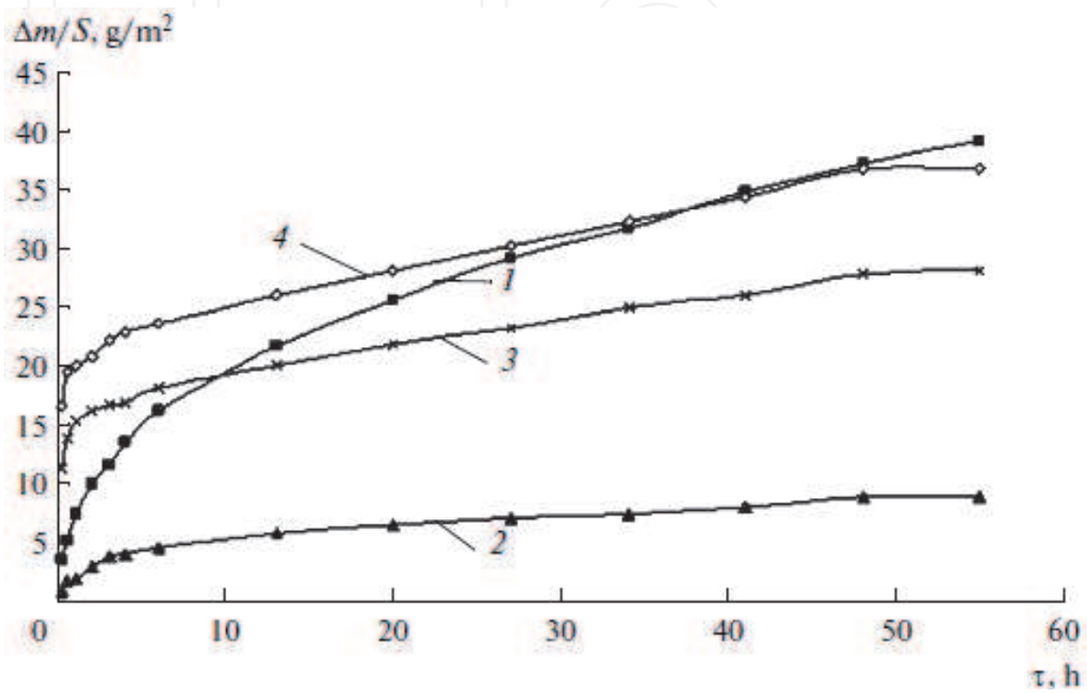

Fig. 18. Oxidation kinetics of the (Ti,Ta)C alloys in air at T = 1073 K. x = 0 (1); 10 (2); 30 (3) , and 50 wt % (4).

The alloy synthesized from the mixture with charging parameter x = 10% showed the highest heat resistance when compared with other ones, including the samples of nonstoichiometric titanium carbide obtained under the same conditions by the SHS compaction technology. The weight increment for this alloy (x = 10%) was < 8 g/m² for 50 h oxidation in air, which exceeds the heat resistance of samples of not only the nonstoichiometric titanium carbide $TiC_{0.5}$, but also stoichiometric TiC and TaC carbides obtained by hot pressing [48]. The alloy with x = 30% under holding > 10 h also has a higher heat resistance than $TiC_{0.5}$. This can be explained by the fact that the samples of nonstoichiometric titanium carbide and complex titanium–tantalum carbide, as a rule, contain a certain amount of α–β-Ti in the first case and β-(Ta,Ti) solid solution possessing higher heat resistance than titanium [75] in the second case.

The higher oxidation rate at short times of holding the samples with a higher tantalum content (x = 30 and 50%) is determined by an increased residual porosity (up to 7%), as well as by the larger extension of grain boundaries due to a decrease in grain size. This facilitates the diffusion of oxygen into the sample depth and increases the weight of formed oxides. The oxidation rate is also affected by protective properties of the oxide film. In our case, oxides appearing on the surface possess strongly differing specific volumes: $V_{Ta_2O_3} / V_{TiO_2} = 1.78$. Therefore, tantalum oxide induces stresses in the oxide film that may lead to a

violation of its integrity, which accelerates oxidation. The tantalum oxide content in the film determines the heat resistance of the alloy. Its small amount affects positively (Fig. 18, curve 2), while heat-resistance drops as it increases (Fig. 18, curves 3, 4). In addition, tantalum carbide is less resistant to high-temperature oxidation than titanium carbide [48].
The oxidation of the alloys follows the logarithmic law: $\Delta m/S = A\ln\tau + B$, where Δm is the difference between the current and initial sample weight, S is the area of the sample surface, and A and B are constant coefficients (Table 13). In this case, the limiting stage of oxidation process is the diffusion through the oxide film.
Generalizing the aforesaid about the Ti–Ta–C system, we can notice that for, compositions with x = 10 and 30 %, an abrupt increase in the combustion rate and temperature is observed at T_0 > 450 K due to the passage from the detached mode to the coalescence mode, which is accompanied by the increment in heat release because of the occurrence of two parallel chemical reactions. For the mixture with x = 50%, the T_0-dependences on T_c and U_c are linear in a wide range of T_0. In the studied range of the mixturing parameter, the products of the synthesis are single-phased and comprise the titanium– tantalum carbide (Ti,Ta)C.

x , wt %	Coefficients of the regression equation	
	A	*B*
0	6.75	7.57
10	1.50	2.32
30	2.90	14.49
50	3.56	19.63

Table 13. Coefficients of the regression equations $\Delta m/S = A\ln\tau + B$

Its lattice constant increases from 0.4304 to 0.4331 nm as x increases from 10 to 50%. The primary structure formation starts in the combustion zone, specifically, submicron grains of nonstoichiometric titanium carbide are allocated from the supersaturated titanium melt. The tantalum particle starts to react only in the aftercombustion zone via the diffusion penetration into the titanium melt and then into the sublattice of nonstoichiometric titanium carbide. The formation of a typical ring structure of grains indicates the primary nucleation of titanium carbide grains and the subsequent dissolution of tantalum (tantalum carbide) in them. An increase in the mixture parameter leads to a decrease in the size and microhardness of the (Ti,Ta)C grains, as well as to a decrease in the relative density of compact synthesis products. The kinetics of high-temperature oxidation is described by the logarithmic equations of the form $\Delta m/S = A\ln\tau + B$. The ceramic obtained at x = 10% has the highest heat resistance.

5. Conclusions

The modern views about the features of the synthesis of few interesting classes of the systems differ in the mechanisms of combustion and structure formation, namely the four-component system $Ti_{2-x}Cr_xAlC$, three-component systems Ti_3AlC_2, Ti_2AlC, Cr_2AlC, the systems based on titanium and chromium borides, and complex titanium–tantalum carbide are considered in this work.

6. Acknowledgment

The experimental works described in the chapter were carried out due to financial support from the Federal Target Program "Scientific and scientific-and-pedagogical personnel of an innovative Russia" for 2009–2013 (State Contracts no. 02.740.11.0133, and 02.740.11.0859), as well as by the Program of creation and development of the National University of Science and Technology "MISIS".

7. References

[1] Levashov, E.A., Shtansky, D.V. (2007). Multifunctional nanostructured films. *Rus. Chem.l Reviews,* Vol. 76, No. 5, p. 463.

[2] Andrievskii, R.A. (2002). Nanomaterials: concept and modern problems. *Ross. Khim. Zh.,* Vol. 46, No. 5, p. 50.

[3] Levashov, E.A., Shtanskii, D.V., Kiryukhantsev-Korneev, F.V., et al. (2009). Mnogofunkcionalnie nanostrukturnie pokritiya: poluchenie, struktura i obespechenie edinstva izmerenii mehanicheskih i tribologicheskih svoistv (Multifunctional Nanostructured Coatings: Preparation, structure and ensuring the measurement of mechanical and tribological properties). *Deform. Razrush.*, No. 11, p. 19.

[4] Shtansky, D.V., Levashov, E.A., Sheveiko, A.N., Moore, J.J. (1999). Optimization of PVD Parameters for the Deposition of Ultra Hard Ti–Si–B–N Coatings. *J. Mater. Synth. Process.*, Vol. 7, No. 3, p. 187.

[5] Musil, J., Jirout, M. (2007). Toughness of Hard Nanostructured Ceramic Thin Films. *Surf. Coat. Technol.,* Vol. 201, p. 5148.

[6] Levashov, E.A., Merzhanov, A.G., and Shtansky, D.V. (2009). Advanced Technologies, Materials and Coatings Developed in Scientific-Educational Center of SHS. *Galvanotechnik,* No. 9, p. 2102.

[7] Sychev, A.E. (2001). *Samorasprostranyayushchiisya vysokotemperaturnyi sintez: teoriya i praktika (Self-Propagating High-Temperature Synthesis: Theory and Practice),* Territoriya, Chernogolovka

[8] Levashov, E.A., Rogachev, A.S., Yukhvid, V.I., Borovinskaya, I.P. (1999). *Fiziko-khimicheskie i tekhnologicheskie osnovy samorasprostranyayushchegosya vysokotemperaturnogo sinteza (Physical-chemical and technological base of the Self-Propagating High-Temperature Synthesis)*, BINOM, Moscow.

[9] Shtansky, D.V., Lyasotsky, I.V., Levashov, E.A., et al. (2004). Comparative Investigation of Ti–Si–N Films Magnetron Sputtered Using Ti_5Si_3 + Ti and Ti_5Si_3 + TiN Targets. *Surf. Coat. Technol.*, Vol. 182, p. 210.

[10] Shtansky, D.V., Kiryukhantsev-Korneev, F.V., Levashov, E.A., et al. (2005) Struktura i svoistva pokritii Ti–B–N, Ti–Cr–B–(N) i Cr–B–(N), poluchennih magnetronnim raspileniem SHS- mishenei (Structure and properties of Ti-B-N, Ti-Cr-B-(N) and Cr-B-(N) coatings, obtained by magnetron sputtering of SHS- targets). *Fiz. Tverd. Tela*, Vol. 47, No. 2, p. 242 [*Phys. Sol. St.* (Engl. Transl.), 2005, Vol. 47, No. 2, p. 252].

[11] Audronis, M., Leyland, A., Levashov, E., et al. (2007). The Structure and Mechanical Properties of Ti–Si–B Coatings Deposited by DC and Pulsed-DC Unbalanced Magnetron Sputtering. *Plasma Process. Polym.*, Vol. 4, p. 687.

[12] Shtansky, D.V., Kulinich, S.A., Levashov, E.A., Moore, J.J. (2003). Osobennosti strukturi i phisico-mehanicheskih svoistv nanostrukturnih tonkih plenok (Features of structure, physical and mechanical properties of nanostructured thin films). *Fiz. Tverd. Tela*, Vol. 45, No. 6, p. 1122 [*Phys. Sol. St.* (Engl. Transl.), Vol. 45, No. 6, p. 1177].

[13] Shtansky, D.V., Levashov, E.A., and Sheveiko, A.N. (1997). Mit einem SHS-Legierungs-Target abgeschiedene Mehrkomponentenschichten Ti–B–N, Ti–Si–B–N, Ti–Si–C–N und Ti–Al–C–N fur unterschiedliche technologische Anwendungen. *Galvanotechnik*, No. 10, p. 3368.

[14] Shtansky, D.V., Kiryukhantsev-Korneev, Ph.V., Levashov, E.A., et al. (2007). Hard tribological Ti–Cr–B–N coatings with enhanced thermal stability, corrosion- and oxidation resistance. *Surf. Coat. Technol.*, Vol. 202, p. 861.

[15] Shtansky, D.V., Lobova, T.A., Levashov, E.A., et al. (2004). Structure and Tribological Properties of WSe_x, WSe_x/TiN, Se_x/TiCN and WSe_x/TiSiN Coatings. *Surf. Coat. Technol.*, Vol. 183, p. 328.

[16] Shtansky, D.V., Sheveyko, A.N., Sorokin, D.I., et al. (2008). Structure and Properties of Nanocomposite and Multilayer TiCrBN/WSe_x Coatings Deposited by Ion Implantation Assisted Sputtering of TiCrB and WSe_2 Targets. *Surf. Coat. Technol.*, Vol. 202, p. 5953.

[17] Kiryukhantsev-Korneev, F.V., Petrzhik, M.I., Levashov, E.A., et al. (2007). Vliyanie Al, Si i Cr na termicheskuyu stabilnost i stoikost k visokotemperaturnomu okisleniyu pokritiy na osnove boronitrida titana (Effect of Al, Si and Cr on the thermal stability and resistance to high temperature oxidation of coatings based on titanium boronitride). *Fiz. Met. Metalloved.,* Vol. 104, No. 2, p. 176.

[18] Paternoster, C., Fabrizi, A., Cecchini, R., et al. (2008). Thermal Evolution and Mechanical Properties of Hard Ti-Cr-B-N and Ti-Al-Si-B-N Coatings. *Sufr. Coat. Technol.*, Vol. 203, p. 736.

[19] Shtansky, D.V., Levashov, E.A., Gloushankova, N.A., et al. (2004). . Structure and Properties of ZrO_2 and CaO-doped TiC_xN_y Coatings for Biomedical Applications. *Surf. Coat. Technol.*, Vol. 182, p. 101.

[20] Shtansky, D.V., Gloushankova, N.A., Bashkova, I.A., et al. (2006). Multifunctional Biocompatible Nanostructured Coatings for Load-Bearing Implants. *Surf. Coat. Technol.*, Vol. 201, p. 4111.

[21] Shtansky, D.V., Gloushankova, N.A., Levashov, E.A., et al. (2006). Multifunctional Ti-(Ca,Zr)-(C,N,O,P) Films for Load-Bearing Implants. *Biomaterials*, Vol. 27, p. 3519.

[22] Shtansky, D.V., Gloushankova, N.A., Levashov, E.A., et al. (2005). Design, characterization and testing of Ti-based multicomponent coatings for load-bearing medical application. *Biomaterials*, Vol. 26, p. 2909.

[23] Shtansky, D.V., Bashkova, I.A., Levashov, E.A., et al. (2008). Bioaktivnie keramicheskie tantalsoderzhashie plenki dlya implantatov (Bioactive ceramic tantal-containing films for implants). *Dokl. Akad. Nauk*, Vol. 418, No. 1, p. 121.

[24] Shtansky, D.V., Gloushankova, N.A., Bashkova, I.A., et al. (2008). Ta-Doped Multifunctional Bioactive Nanostructured Films. *Sufr. Coat. Technol.*, Vol. 202, p. 615.

[25] Zhong, D., Sutter, E., Levashov, E.A., et al. (2001). Mechanical properties of Ti–B–C–N coatings deposited by magnetron sputtering. *Thin Solid Films*. Vol. 398–399, p. 320.

[26] Kulisch, W., Colpo, P., Gibson, P.N., et al. (2004). ICP assisted sputter deposition of TiC/CaO nanocomposite films. *Surf. Coat. Technol.*, Vol. 188–189, p. 735.

[27] Werner, Z., Stanislawski, J., Levashov, E., et al. (2003). New Types of Multi-Component Hard Coatings Deposited by ARC PVD on Steel Pre-treated by Pulsed Plasma Beams. *Vacuum*, Vol. 70, pp. 263.

[28] Kiryukhantsev-Korneev, F.V., Shtansky, D.V., Levashov, E.A., et al. (2004) Struktura i svoistva Ti–Si–N pokritii, poluchennih magnetronnim raspileniem SHS- mishenei (Structure and properties of Ti-Si-N coatings deposited by magnetron sputtering of SHS targets). *Fiz. Met. Metalloved.*, Vol. 97, No. 3, p. 96.

[29] Shtansky, D.V., Levashov, E.A., Sheveiko, A.N., Moore, J.J. (1998). The Structure and Properties of Ti–B–N, Ti–Si–B–N, Ti–Si–C–N and Ti–Al–C–N coatings deposited by magnetron sputtering using composite targets produced by self-propagating High-temperature Synthesis (SHS). *J. Mater. Synth. Process.*, Vol. 6, No. 1, p. 61.

[30] Shtansky, D.V., Sheveiko, A.N., Levashov, E.A., et al. (2005). Hard Tribological Ti–B–N, Ti–Cr–B–N, Ti–Si–B–N and Ti–Al–Si–B–N Coatings. *Surf. Coat. Technol.*, Vol. 200, p. 208.

[31] Shtansky, D.V., Levashov, E.A., Khavskii, N.N., Moore, J.J. (1996). Perspektivi sozdaniya kompozitnih iznosostoikih plenok, poluchaem ih s ispolzovaniem SHS-katodov (Prospects of wear-resistant composite films deposition using SHS cathodes). *Izv. Vyssh. Uchebn. Zaved., Tsvetn. Metall.*, No. 1, p. 59.

[32] Shtansky, D.V., Kaneko, K., Ikuhara, Y., Levashov, E.A. (2001). Characterization of Nanostructured Multiphase Ti–Al–B–N Thin Films with Extremely Small Grain Size. *Surf. Coat. Technol.*, Vol. 148, p. 206.

[33] Kiryukhantsev-Korneev, Ph.V., Pierson, J.F., Levashov, E.A., et al. (2009). Effect of Nitrogen Partial Pressure on the Structure, Physical and Mechanical Properties of CrB2 and Cr–B–N films. *Thin Solid Films*, Vol. 517, p. 2675.

[34] Kiryukhantsev-Korneev, Ph.V, Pierson, J.F, Bauer, J.P., Levashov, E.A., et al. (2008). Structure and Properties of Hard Nanostructured Coatings in Cr-B-N system, *Proceedings of the III France–Russia Seminar "New Achievements in Materials and Environmental Sciences"*, Paris: EDP Sciences, 2008, p. 11.

[35] Shtansky, D.V., Kiryukhantsev-Korneev, F.V., Levashov, E.A., et al. (2010). Multicomponent Nanostructured Films for Various Tribological Applications. *Int. J. Refract. Met. Hard Mater.*, Vol. 28, p. 32.

[36] Shtansky, D.V., Kiryukhantsev-Korneev, F.V., Levashov E.A., et al. (2009). Comparative Investigation of TiAlC(N), TiCrAlC(N) and CrAlC(N) Coatings Deposited by Sputtering of MAX- phase $Ti_{2-x}Cr_xAlC$ Targets. *Surf. Coat. Technol.*, Vol. 203, p. 3595.

[37] Barsoum, M.W. and El-Raghy, T. (2001). The MAX Phases: Unique New Carbide and Nitride Materials. *Am. Sci.*, Vol. 89, No. 4, p. 11.

[38] Eklund, P., Beckers, M., Jansson, U., et al. (2010). The $M_{n+1}AX_n$ phases: Materials Science and Thin-Film Processing. *Thin Solid Films*, Vol. 518, p. 1851.

[39] Tzenov, N.V., Barsoum, M.W. (2000). Synthesis and Characterization of Ti_3AlC_2. *J. Am. Ceram. Soc.*, Vol. 83, No. 4, p. 825.

[40] Wubian Tian, Peiling Wang, Guojun Zhang et al. (2006). Synthesis and thermal and electrical properties of bulk Cr_2AlC. *Scr. Mater.*, Vol. 54. p. 841.

[41] Levashov, E.A., Pogozhev, Yu.S., Shtansky, D.V., Petrzhik, M.I., (2009). Self-Propagating High-Temperature Synthesis of Ceramic Materials Based on the $M_{n+1}AX_n$ Phases in the Ti-Cr-Al-C System. *Russ. J. Non-Fer. Met.*, Vol. 50, No. 2, p. 151.

[42] Zhimei, Sun., Rajeev, Ahuja, Jochen, M. Shnaider. (2003). Theoretical investigation of the solubility in $M_xM'_{2-x}AlC$ (M and M' are Ti,V,Cr). *Phys. Rev. B*, Vol. 68, p. 4.

[43] Zou, Y., Sun, Z.M., Tada, S., and Hashimoto, H. (2006). *Scr. Mater.*, Vol. 55, p. 767.

[44] Levashov, E.A., Kurbatkina, V.V., Rogachev, A.S., Kochetov, N.A. (2007). Mechanoactivation of SHS Systems and Processes. Int. Journal of Self-Propagating High-Temperature Synthesis. *Int. J. SHS, 2007*, Vol. 16, No. 1, p. 46.

[45] Kurbatkina, V.V, Levashov, E.A, and Rogachev, A.S, (2007). Mechnoactivation of SHS. In: *Combustion of Heterogeneous Systems: Fundamentals and Application for Materials Synthesis*, Mukasyan A.S., Martirosyan, K.S., p. 131–143, Transword Research Network.

[46] Kurbatkina, V.V., Levashov, E.A., Patsera, E.I., et al. (2009). Issledovanie macrokineticheskih harakteristic processov goreniya predvaritelno mehanicheski aktivirovannih reakcionnih smesei Cr-B i Cr-Ti-B (Study of the macrokinetic characteristics of combustion processes of previously mechanically activated Cr-B and Cr-Ti-B reaction mixtures). *Khim. Interesakh Ustoich. Razvit.*, No. 6, p. 21.

[47] Kochetov, N.A., Rogachev, A.S., Pogozhev, Yu.S. (2010). The effect of mechanical activation of a reaction mixture on the velocity of the wave propagation of SHS reactions and microstructure of the TiC–Ni hard alloy. *Russ. J. Non-Fer. Met.*, Vol. 51, No. 2, p. 177.

[48] Voitovich, R.F., Pugach, E.A., (1978). *Okislenie tugoplavkikh soedinenii: Spravochnik (Oxidation of Refractory Compounds: Handbook)*, Metallurgiya, Moscow.

[49] Samsonov, G.V., Markovskii, L.Ya., Zhigach, A.F., Valyashko, M.G. (1960). *Bor, ego soedineniya i splavy (Boron, Its Compounds and Alloys)*, Kiev: AN USSR.

[50] Okada, S., Kudou, K., Iisumi, K., et al. (1996). Single-crystal growth and properties of CrB, Cr_3B_4, Cr_2B_3 and CrB_2 from high-temperature aluminum solutions. *J. Cryst. Growth*, Vol. 166, p. 429.

[51] Muetterties, E.L. (1976). *The Chemistry of Boron and Its Compounds*, Wiley, New-York.

[52] Samsonov, G.V., Serebryakova, T.I., and Neronov, V.A. (1975). *Boridy (Borides)*, Atomizdat, Moscow.

[53] Kuz'ma, Yu.B. (1983). *Kristallokhimiya boridov (Crystal Chemistry of Borides)*, Vyshcha Shkola, Lviv.

[54] Kosolapova, T.Ya. (1986). Svoistva, poluchenie i primenenie tugoplavkikh soedinenii: Spravochnik (Properties, Obtaining, and Application of Refractory Compounds: Handbook), Metallurgiya, Moscow.

[55] Serebryakova, T.I., Neronov, V.A., Peshev, P.D. (1991). *Vysokotemperaturnye boridy (High-Temperature Borides)*, Metallurgiya, Chelyabinsk.

[56] Ivanovskii, A.L., Shveikin, G.P. (1998). *Kvantovaya khimiya v materialovedenii. Bor, ego splavy i soedineniya (Quantum Chemistry in Materials Science. Boron, Its Alloys and Compounds)*, UrO RAN, Yekaterinburg.

[57] Levashov, E.A., Kurbatkina, V.V., Patsera, E.I., et al. (2008). Combustion and structure formation in the mechanoactivated Cr-B system. *Int. J. SHS*, Vol. 17, No. 3, p. 189.

[58] Eremina, E.N., Kurbatkina, V.V., Levashov, E.A., et al. (2005). Poluchenie compositsionnogo materiala MoB metodom silovogo SHS- kompaktirovaniya s primenenirm mehanicheskogo aktivirovaniya ishodnoi smesi Mo-10%B (Obtaining of MoB composite material by forced SHS- pressing with using of preliminary mechanical activation of the initial mixture of Mo-10%B). *Khim. Interesakh Ustoich. Razvit.*, Vol. 13, p. 197.

[59] Avakumov, E.G. (2009). *Fundamental'nye osnovy mekhanicheskoi aktivatsii, mekhanosinteza i mekhanokhimicheskikh tekhnologii: Sbornik statei (Fundamental Base of Mechanical Activation, Mechanosynthesis, and Mechanochemical Technologies: Collected Articles)*, SO RAN, Novosibirsk.

[60] Lyakhov, N.Z., Talako, T.L., Grigoreva, T.F. (2008). *Vliyanie mekhanoaktivatsii na protsessy fazo- i strukturoobrazovaniya pri samorasprostranyayushchemsya vysokotemperaturnom sinteze (Influence of the Mechanical Activation on the Structure Formation during the Self-Propagating High-Temperature Synthesis)*, Parallel, Novosibirsk.

[61] Grigoreva, T.F., Barinova, A.P., Lyakhov, N.Z. (2008). *Mekhanokhimicheskii sintez v metallicheskikh sistemakh (Mechanochemical Synthesis in Metallic Systems)* (Avakumov, E.G. edition), Parallel, Novosibirsk.

[62] Novikov, I.I., Rozin, K.M. (1990). *Kristallografiya i defekty kristallicheskoi reshetki (Crystallography and Defects of Crystal Lattice)*, Metallurgiya, Moscow.
[63] Boldyrev, V.V., Tkasova, A.K. (2000). Mechanochemistry of solids: Past, present, and prospects. *J. Mater. Synth. Process*, Vol. 8, No. 3–4, p. 121.
[64] Shelekhov, E.V., Pripisnov, O.N., Rupasov, S.I. (2001). Analiz tonkoi strukturi Cr v processe mehanicheskogo aktivirovaniya smesei Cr-C (Analysis of the thin structure of Cr during mechenical activation of the Cr-C mixtures). *Izv. Vyssh. Uchebn. Zaved., Tsvetn. Metall.*, No. 1, p. 29.
[65] Gorelik, S.S., Rastorguev, L.N., Skakov, Yu.A. (1999). Rentgenograficheskii i elektronno-opticheskii analiz (X-Ray Diffraction and Electron-Optical Analyses), MISiS, Moscow.
[66] Levashov, E.A., Rogachev, A.S., Epishko, Yu.K., Kochetov, N.A. (2007). Samorasprostranyayushiisya visokotemperaturnii sintes katodov-mishenei v sisteme Ti-Ta-C-$Ca_3(PO_4)_2$ dlya ionno-plazmennogo napileniya mnogofunkcionalnih biosovmestimih pokritii (Self-propagating high-temperature synthesis of target cathodes in the system Ti-Ta-C-$Ca_3(PO_4)_2$ for the ion-plasma deposition of multifunctional biocompatible nanostructured coatings). *Izv. Vyssh. Uchebn. Zaved., Poroshk. Metall. Funkts. Pokr.*, No. 1, p. 14.
[67] Mossino, P. (2004). *Ceram. Int.*, Vol. 30, No. 3, p. 311.
[68] Rogachev, A.S., Mukasyan, A.S., and Merzhanov, A.G. (1987). Strukturnie prevrasheniya pri bezgazovom gorenii sistem titan-uglerod i titan-bor (Structural transformations during gasless combustion of titanium-carbon and titanium-boron systems.) *Dokl. Akad. Nauk*, Vol. 297, No. 6, p. 1425.
[69] Levashov, E.A., Kurbatkina, V.V., Rogachev, A.S., et al. (2008). Characteristic properties of combustion and structure formation in the Ti–Ta–C system. *Rus. J. Non-Fer. Met.,* Vol. 49, No. 5, p. 404
[70] Merzhanov, A.G., Mukasyan, A.S. (2007). *Tverdoplamennoe gorenie (Solid-State Combustion),* TORUS PRESS, Moscow.
[71] Levashov, E.A., Senatulin, B.R., Leyland, A., Matthews, A. (2006). *Rus. J. Non-Fer. Met.*, Vol. 47, No. 1, p. 39.
[72] Merzhanov, A.G. (1979). Processi goreniya kondensirovannih sistem. Novoe napravlenie issledovanii (Combustion of condensed systems. The new direction of research). *Vestn. Akad. Nauk SSSR*, No. 8, p. 10.
[73] Pearson, W.B. (1958). *Handbook of Lattice Spacings and Structures of Metals and Alloys*, Pergamon, New York.
[74] Kiparisov, S.S., Levinskii, Yu.V., Petrov, V.M. (1989). *Karbid titana (Titanium Carbide)*, Metallurgiya, Moscow.
[75] Kubashewsky, O., Hopkins, B. (1969). *Okislenie metallov i splavov (Oxidation of Metals and Alloys)*, Mir, Moscow.

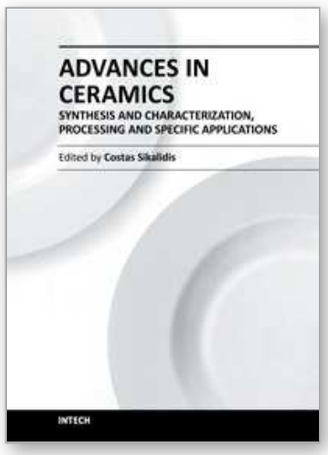

Advances in Ceramics - Synthesis and Characterization, Processing and Specific Applications

Edited by Prof. Costas Sikalidis

ISBN 978-953-307-505-1
Hard cover, 520 pages
Publisher InTech
Published online 09, August, 2011
Published in print edition August, 2011

The current book contains twenty-two chapters and is divided into three sections. Section I consists of nine chapters which discuss synthesis through innovative as well as modified conventional techniques of certain advanced ceramics (e.g. target materials, high strength porous ceramics, optical and thermo-luminescent ceramics, ceramic powders and fibers) and their characterization using a combination of well known and advanced techniques. Section II is also composed of nine chapters, which are dealing with the aqueous processing of nitride ceramics, the shape and size optimization of ceramic components through design methodologies and manufacturing technologies, the sinterability and properties of ZnNb oxide ceramics, the grinding optimization, the redox behaviour of ceria based and related materials, the alloy reinforcement by ceramic particles addition, the sintering study through dihedral surface angle using AFM and the surface modification and properties induced by a laser beam in pressings of ceramic powders. Section III includes four chapters which are dealing with the deposition of ceramic powders for oxide fuel cells preparation, the perovskite type ceramics for solid fuel cells, the ceramics for laser applications and fabrication and the characterization and modeling of protonic ceramics.

InTech Europe
University Campus STeP Ri
Slavka Krautzeka 83/A
51000 Rijeka, Croatia
Phone: +385 (51) 770 447

InTech China
Unit 405, Office Block, Hotel Equatorial Shanghai
No.65, Yan An Road (West), Shanghai, 200040, China
中国上海市延安西路65号上海国际贵都大饭店办公楼405单元
Phone: +86-21-62489820

Fax: +385 (51) 686 166
www.intechopen.com

Fax: +86-21-62489821

IntechOpen